UNIVERSITÀ DEGLI STUDI DI MILANO

SCUOLA DI SPECIALIZZAZIONE IN NEUROLOGIA

Multimodal Magnetic Resonance Imaging for the identification of early Multiple System Atrophy biomarkers

Relatore: Chiar.mo Prof. Vincenzo Silani

Correlatore: Prof. Nicola Pavese

Tesi di specializzazione di:

Jacopo Pasquini

Matricola: S61764

Anno accademico 2019/2020

Table of contents

Acknowledgement

A special *thank you* to otherwise unnamed contributors of this project: Victoria Foster, Dr Laura Best and Dr Michael Firbank (in random order) for their work in data collection and neuroimaging analysis.

A special *thank you* to the Multiple System Atrophy Trust and Parkinson's UK for providing funding for all research activities related to subjects' participation, and to the Clinical Ageing Research Unit and the Centre for In Vivo Imaging, Newcastle University where the research tool place.

A special *thank you* to the European Academy of Neurology for awarding me with a research fellowship grant that made this thesis possible.

I declare no competing interests related to the content presented in this thesis.

Summary

Background. Multiple system atrophy (MSA) is a rare, sporadic disease characterized by autonomic failure and a various combination of parkinsonism and cerebellar dysfunction. Currently, development of new treatment strategies in MSA is hampered by the lack of reliable diagnostic and disease-progression biomarkers. The aim of this study was to investigate brain microstructural abnormalities in MSA through diffusion and neuromelanin-sensitive magnetic resonance imaging (MRI) and their relationship with clinical manifestations.

Methods. Clinical evaluation and MRI were performed on 11 MSA patients, 19 Parkinson's Disease (PD) and 18 healthy controls (HC). MRI scans included structural, diffusion (dMRI) and neuromelanin-sensitive sequences. dMRI was applied through a novel technique, neurite orientation dispersion and density imaging (NODDI). Compared to previous dMRI techniques, NODDI allows the simultaneous evaluation of the integrity of the intracellular and extracellular compartments, while gathering information on the orientation of axons and dendrites. Neuromelanin-sensitive MRI was used to quantitively investigate the integrity of substantia nigra (SN) and locus coeruleus (LC).

Results. Median duration of symptoms in MSA patients was 3 years (range 1-6). Age was not significantly different across subgroups. Compared to PD, MSA patients had reduced neurite density index (NDI) in the middle cerebellar peduncle (MCP) and in the pons (Mann-Whitney U=44.0, p=0.019 and U=52.0, p=0.050), indicating white matter degeneration in these locations, and increased free water fraction (FWF), indicating grey matter loss, in the putamen, caudate and cerebellar lobule VI grey matter (U=146.0, p=0.019; U=145.0, p=0.021; U=154.0, p=0.006 respectively). Neuromelanin content was not different in SN and LC between PD and MSA, although this was reduced in the posterior SN and intermediate part of LC compared to HCs (Kruskal Wallis H=11.363, p=0.003 and H=13.788, p=0.001),

indicating similar, significant degeneration of these nuclei in both conditions. No significant correlations were found between motor scores and MRI parameters in the SN, putamen, and MCP and pons. LC neuromelanin loss in the rostral and/or intermediate sections was significantly associated with greater cognitive, depressive and REM sleep behaviour disorder (RBD) symptoms scores in MSA. Symptoms of dysautonomia were not associated with diffusion or neuromelanin content measures.

Conclusion. Multimodal MRI with diffusion and neuromelanin evaluation may help define structural abnormalities in the early stages of MSA. NODDI seems a promising technique to simultaneously evaluate multiple microstructural parameters in critical locations of MSA pathology, such as the basal ganglia, cerebellum, and pons. Neuromelanin content evaluation is useful for defining SN and LC degeneration, although this occurs similarly in MSA and PD. In MSA, LC degeneration is associated with greater depressive, cognitive and RBD symptoms. Longitudinal investigations are needed to establish whether these MRI parameters may serve as disease-progression biomarkers.

Introduction

Multiple system atrophy (MSA) is a neurodegenerative disorder characterized by autonomic failure and a variable combination of ataxia, parkinsonism and pyramidal signs.[1] Depending on the predominant phenotype, either ataxic or parkinsonian, MSA can be further subdivided into cerebellar (MSA-C) and parkinsonian (MSA-P). The neuropathological hallmark of MSA is argirophilic oligodendro-glial cytoplasmic inclusions (GCIs)[2] containing aggregates of insoluble α-synuclein.[3] Oligodendroglial pathology is in turn associated with myelin pallor and degeneration, and neuronal loss; microglial activation and astrogliosis also occur.[4,5] GCIs can be found throughout the brain. Their highest density has been reported in the basal ganglia and especially in the highly myelinated striatopallidal fibers (Wilson pencil fibers) of the putamen,[6] and the density of CGIs is associated with neuronal loss.[4] The areas affected by prominent demyelination and neuronal loss are the central autonomic nuclei (e.g. hypothalamus, rostral ventrolateral medulla, intermediolateral column of the spinal cord) the basal ganglia (putamen, pallidus, substantia nigra) and the olivo-ponto-cerebellar system (inferior olivary nucleus, pontine fibers, middle cerebellar penducles and cerebellum)[7]. The severity of pathologic abnormalities in each system is associated with autonomic, parkinsonian and cerebellar symptoms.[8] Neuronal cytoplasmic and intranuclear inclusions and dystrophic neurites are also found in grey matter (e.g. substantia nigra, basal ganglia, inferior olivary nucleus, limbic cortex, hypotahalamus), although their clinical significance is unclear.[9]

In the early stages, MSA can be clinically indistinguishable from Parkinson's Disease (PD), especially when presenting with prominent parkinsonian features. PD is a neurodegenerative alpha-synucleinopathy with different pathological and progression characteristics. Indeed, the pathological hallmark of PD is alpha-synuclein accumulation in Lewy bodies (LB) inside the neuronal cytoplasm and neurites (dystrophic Lewy neurites).[10] While the progression of MSA

to significant degrees of disability is rapid, that of PD is variable but usually slower. While PD patients usually maintain their functional independence for more than 10 years with appropriate management, MSA patients have an estimated average 6.7 years from disease onset to wheelchair dependency.[11,12] Furthermore, treatment strategies in MSA are currently limited to management of symptoms with many shortcomings.[13] Therefore, the detection of early biomarkers is critical in MSA for the development of symptomatic and disease-modifying strategies.

In this thesis project, magnetic resonance imaging (MRI) was used to investigate early microstructural abnormalities in MSA as possible disease and pathophysiological biomarkers.

MRI brain microstructural abnormalities in MSA

In this section, imaging modalities relevant to this project, i.e. diffusion MRI (dMRI) and neuromelanin-sensitive MRI, will be reviewed.

General principles of diffusion MRI

Diffusion MRI describes the physiological characteristics of water molecules random movements (Brownian motion). Since brain tissue is inhomogeneous and water separated in different compartments, diffusion MRI can infer brain structure characteristics based on the diffusion properties of water molecules. In brain imaging, the first application of these principles was diffusion-weighted imaging (DWI), an MRI technique capable of generating images with signal intensities sensitized to water random motion.[14] From a series of DW images (e.g. two series acquired with different diffusion weighting, i.e. b-values) it is possible to calculate an apparent diffusion coefficient (ADC) of water molecules. The ADC at each pixel can be mapped to create an ADC image. The ADC is derived from an acquisition

technique that allows measuring the displacement of water molecules in one axis only. Therefore, measuring diffusion along 3 orthogonal axes (e.g. x, y, z) will produce three images with different contrasts; the contrast of these three images is therefore orientation-dependent.[15] This property constitutes a significant limitation in the study of the human brain, where neighbouring fibre bundles may be oriented in different directions. The orientation-dependent effect is generated by the preferential directionality of water diffusion in the human brain, a phenomenon called diffusion anisotropy.[16] Diffusion anisotropy is a consequence of the strict water compartmentalization in living systems. A stark example of this phenomenon is water inside axons, where it diffuses preferentially along its main axis, while its movement is highly restricted transversally by cell membranes and myelin sheaths. Conversely, freely diffusing water is characterized by isotropic movements, i.e. no preferential directionality. To overcome the limitations of the ADC parameter, a new modelling of diffusion imaging was proposed, named diffusion tensor imaging (DTI). In each voxel, DTI represents anisotropic diffusion through an ellipsoid that can be mathematically modelled by a 3x3 matrix, named tensor, as opposed to the ADC that represents diffusion in a voxel with a single value.[17] This model allows representing the diffusion of water molecules in three-dimensional space, describing the different directions and "strengths" of the movement. DTI analysis enables to infer the molecular diffusion rate with parameters such as mean diffusivity (MD) or, again, ADC; the diffusion rate along the main axis and transverse axis of diffusion, axial diffusivity (AD) and radial diffusivity (RD) respectively; the preferential directionality of diffusion, fractional anisotropy (FA). Anisotropy is expressed as a relative fractional value between 0 and 1. As a reference example, diffusion in white matter is preferential along the axons and therefore highly anisotropic, in grey matter diffusion is less anisotropic, and in the cerebrospinal fluid (CSF) water movement is unrestricted, i.e. isotropic.[18]

Table 1 shows a selection of concepts related to diffusion imaging that will allow a deeper understanding of the results of the studies reported.[19–22]

Neurite orientation dispersion and density imaging (NODDI)

NODDI investigates tissue microstructure through diffusion MRI. As opposed to conventional DTI, NODDI is based on acquisition of diffusion gradients of different strengths to provide more specific indices of tissue microstructure.[22] NODDI models brain tissue using a biophysical model that identifies three types of microstructural environments: intra-neurite, extra-neurite, and cerebrospinal fluid (CSF) compartments. This is achieved by applying a two-level approach to separate the volume fraction of Gaussian isotropic diffusion (isotropic volume fraction, ISOvf, or free water fraction, FWF), representing freely diffusing water (i.e. CSF), from the remaining brain tissue. The remaining signal is compartmentalised into non-exchanging intra and extra-neurite water. This model provides important markers: the neurite density index (NDI, or intracellular volume fraction, ICvf), i.e. the fraction of diffusing water compartmentalised inside neurites (axons and possibly dendrites); the orientation dispersion index (ODI) which reflects the spatial configuration of the neurites; and the free water fraction (FWF, or isotropic volume fraction, ISOvf) representing the portion of extracellular, freely diffusing water. A schematic representation of the NODDI tissue modelling is shown in **Figure 1**.[23]

According to this orientation-dispersed cylindric model, the isotropic diffusion fraction is highly represented only within CSF, whereas within brain parenchyma, the diffusion signal can be either hindered (Gaussian displacement pattern) or restricted (non-Gaussian displacement pattern). The restricted signal is attributed to intraneurite spaces and is corresponds to the neurite density index (NDI). The hindered signal is attributed to the extra-

neurite compartment, which encompasses everything except neurites and free water, such as microglia, astrocytes, oligodendrocytes, neuronal cell bodies (somas), ependymal cells, extra-cellular matrices, and vascular structures. A Watson distribution is then used to compute the orientation distribution of the cylinders, quantified from 0 to 1 by the orientation dispersion index (ODI).[22] Thus, large ODI values correspond to highly dispersed neurites (e.g. grey matter) and small values to highly aligned axons (e.g. white matter tracts).

Diffusion MRI in MSA

Diffusion MRI has been used in MSA to investigate brain microstructural abnormalities and to establish diagnostic and disease progression biomarkers. Diffusion abnormalities have been found in MSA critical regions such as the middle cerebellar peduncle (MCP), pontine white matter and putamen[24–27]. However, microstructural abnormalities have been described diffusely in white matter: along the pyramidal tract (to a similar extent of patients with amyotrophic lateral sclerosis[28]), in the left premotor cortex[29], periputaminal white matter[30], anterior thalamic radiation[31], corpus callosum[32], afferent and efferent cerebellar white matter.[33] One study showed that whole-brain white-matter mean diffusivity was significantly increased in MSA compared to PD, indicating widespread white matter degeneration throughout the brain.[34] A recent study assessed white matter integrity in MSA-C and sporadic adult-onset ataxia (SAOA), two entities that pose significant challenges in terms of differential diagnosis, especially early in the disease course. It was shown that MSA-C have reduced fractional anisotropy in the pons and cerebellum and along the cortico-spinal tract compared to SAOA[35].

Grey matter has also been assessed in MSA through DTI. Putamen mean diffusivity is increased in MSA compared to PD[36,37] and this is inversely correlated with glucose

metabolism detected with 18-flurodeoxyglucose (^{18}FDG) positron emission tomography (PET)[36]. One study employed free water as a measure of the degree of grey matter neurodegeneration in multiple brain locations.[38] Free water is estimated from dMRI using a bicompartmental model of water diffusion, i.e. a compartment with restricted diffusion and a compartment with unrestricted diffusion (isotropic compartment).[20] It has been shown that an increase in the free water compartment in critical grey matter regions may be related to neurodegeneration.[39–41] In MSA, an increase in free water compared to PD was shown in putamen, caudate, red nucleus, thalamus and several other regions.[38]

Diffusion MRI has also been used to investigate its possible diagnostic applications. Putaminal regional apparent diffusion coefficient (rADC), a measure of microstructural abnormalities, was found increased in MSA-P compared to PD and provided optimal accuracy in discriminating between the two groups.[24–26,42,43] MCP, cerebellar and pontine white matter also showed increased rADC, in both MSA-C[44] and MSA-P[26,45], indicating the presence of white matter structural abnormalities in both subtypes. Trace(D) values, a more accurate index of water diffusion, was also increased in putamen and middle cerebellar peduncles of MSA-P compared to PD patients[46,47]. Interestingly, Trace(D) values were increased in the posterior putamen compared to the anterior putamen[27,46], a finding that is in agreement with the pathological observation of a greater degree of neuronal degeneration in the posterior putamen[48]. Furthermore, Trace(D) also demonstrated the potential as longitudinal biomarker, since values were shown to increase significantly in the putamen[49], cerebellar white matter, and frontal white matter over time.[50] Regional ADC and Trace(D) values of putamen and MCP were also compared against single photon emission tomography (SPECT) measures in terms of diagnostic accuracy. One study found that striatal rADC values performed better than post-synaptic D2 receptor imaging with ^{123}iodobenzamide (^{123}IBZM) SPECT[42] in distinguishing MSA-P from PD; another study showed that putaminal

Trace(D) values were more accurate than ^{123}I-metaiodobenzylguanidine (mIBG) cardiac SPECT.[47] A similar study in patients with a shorter disease duration (<3 years) revealed comparable specificity and lower sensitivity for mIBG cardiac scintigraphy (48% vs 75%).[51]

More recently, machine learning algorithms based on sets of regions of interest were used to classify PD, MSA and progressive supranuclear palsy patients with high accuracies.[52–54]

Neuromelanin-sensitive MRI

Neuromelanin (NM) is an insoluble dark pigment that consists of melanin, proteins, lipids, and metal ions.[55] It is synthesized by iron-dependent oxidation of catecholamines such as dopamine and norepinephrine[56] and it accumulates in specific organelles together with iron and lipids.[57] These organelles increase with aging and are thought to have a very slow turnover.[55] The neuromelanin-iron complexes have paramagnetic properties and may therefore be visualized through MRI.[58] Neuromelanin produces hyperintense signal in neuromelanin-rich nuclei such as the substantia nigra (SN) or the locus coeruleus (LC); this effect is due to the short longitudinal relaxation time (T1) of the neuromelanin complexes and the magnetization effect of the surroundings[59], which can be boosted by a magnetization pulse that enhances the visualization contrast of neuromelanin-containing neurons.[60] The trajectory of neuromelanin concentration with age has been shown with MRI, displaying a strong increase from childhood to adolescence, a plateau through middle age and a decline in older age; a higher concentration in females over 47 years of age was also shown compared to males.[61] Furthermore, neuromelanin content estimated through MRI has been shown to have the potential to represent variations in SN dopaminergic function, not only in neurodegeneration, but also in normal individuals and patients with psychosis.[62] Another study showed that the post-mortem number of SN neuromelanin containing cells was highly

correlated with previous in vivo measurement of DAT availability in a small sample of heterogeneous parkinsonian patients (PD, MSA, DLB, CBD).[63]

In PD, in vivo neuromelanin content is reduced in both the SN (posterior > anterior) and in the LC compared to controls.[58,64] Nigral neuromelanin content has also shown an inverse association with motor impairment.[64,65] Similar reductions have also been found in MSA.[66–69] The diagnostic value of this technique is however still debated, since these studies showed variable degree of overlapping values between MSA and PD. Instead, a recent visual and quantitative analysis of showed that most MSA-P patients had normal SN size and signal intensity and normal LC signal, a pattern substantially different from idiopathic PD.[70]

LC integrity has been associated with better cognitive performances in older adults[71] and LC signal loss has been associated with worse cognitive performances in PD patients.[65,72] It is currently unknown whether motor and non-motor symptoms are associated with loss of neuromelanin signal in the SN and LC in MSA.

Aim of the study

The aims of this study are: i) to investigate differences in diffusion and neuromelanin parameters between MSA patients, PD patients and healthy controls in critical cerebral regions such as the basal ganglia, the pontine and cerebellar regions; ii) to investigate the presence of any association between diffusion and neuromelanin parameters related to neurodegeneration in the substantia nigra; iii) to establish clinical correlates of microstructural abnormalities investigated through diffusion and neuromelanin MRI.

Methods

Participants

Participants enrolled in this study were recruited from the Newcastle upon Tyne NHS Clinics for Research and Service in Themed Assessment (CRESTA, Campus for Ageing and Vitality, Westgate Road, Newcastle Upon Tyne, Tyne And Wear, NE4 6BE) among patients attending the Movement Disorders clinics and their healthy non-first-degree relatives. Age between 45 and 80 was an inclusion criterion for all participants. Additionally, healthy controls (HC) were required to show no clinical neurological dysfunction or MRI structural brain abnormalities; MSA patients had to have a diagnosis of MSA according to current consensus criteria[1]; PD patients were required to have a diagnosis of PD according to UK Brain Bank Criteria.[73] Eleven patients with a probable or possible diagnosis of MSA (7 with predominant parkinsonian features and 4 with predominant cerebellar features), 19 patients with PD and 18 healthy controls concluded the study. Exclusion criteria for all participants were: a diagnosis of other forms of atypical parkinsonism, significant memory impairment (MMSE<24 at screening visit) or meeting DSM V criteria for major neurocognitive disorder, contraindications to MRI or PET scan, people with severe comorbid illness as judged by the investigator.

Clinical Assessments

All participants underwent the following clinical assessment on the day of the MRI scan: Mini Mental State Examination (MMSE) and REM Sleep Behaviour Disorder Questionnaire (RBDSQ). Both MSA and PD patients underwent: Movement Disorders Society – Unified Parkinson's Disease Rating Scale (MDS-UPDRS) sections I and II, Montreal Cognitive Assessment (MoCA), Hospital Anxiety and Depression Scale (HADS), Scales Related to

Outcomes in Parkinson's disease (SCOPA): autonomic dysfunction (SCOPA-AUT), sleep (SCOPA-SLEEP), psychosocial functioning (SCOPA-PS); and the Non-Motor Symptoms Questionnaire (NMSQ). MSA patients only were evaluated with the Unified Multiple System Atrophy Rating Scale (UMSARS) parts I, II and III, while in PD patients motor signs were evaluated with the MDS-UPDRS part III.

MRI acquisition

All images were acquired on a 3T PET-MR System (Signa, GE Healthcare, Milwaukee, WI).

A T1 weighted 3D was acquired through a sagittal fast spoiled gradient recall (FSPGR) sequence with inversion time 400ms, echo time = 3 ms, TR flip angle = 11° voxel size 1x1x1 mm and parallel acceleration factor = 2.

Axial T2 weighted images were acquired through a spin echo sequence, with TR 4375 ms, TE 78 ms, echo train length = 12. 48 slices (3 mm) were acquired with a field of view 240 x 240 and an acquisition matrix 256 x 256.

Diffusion MRI

Multi-shell diffusion weighted Echo Planar Imaging (EPI) was performed with repetition time (TR) 5500 ms, echo time (TE) 102. Multi-shell diffusion weighting was achieved with b-values = 0 (n = 10), 300 (n = 8), 700 (n = 30) and 2000 s/mm2 (n = 60). 74 slices of 2.2 mm were acquired, with field of view 220 x 220 mm and acquisition matrix 100x100. Parallel acceleration factor = 2 and multiband acceleration factor = 3 were used. One volume with b-value=0 and reverse phase encoding direction was also collected.

Neuromelanin MRI

Two types of neuromelanin-sensitive acquisitions were performed. The decision to use two different sequences for the identification of SN and LC was based on previous studies indicating better contrast for either one (e.g. the SN[74]) and previous experience with the PET-MR scanner used for this study.

An axial magnetisation-transfer prepared (MT) 2D gradient echo-based (GRE) sequence, as in Langley et al.[75], was performed through with TR = 500 ms, TE = 4.2 ms, flip angle = 50°; magnetisation frequency offset = 1200 Hz, flip angle = 300°. 13 slices (2.5 mm + 0.3mm gap) were acquired with field of view 220 x 165 mm and acquisition matrix 512 x 384. Two acquisitions were performed.

The second type of acquisition was based on a fast spin echo (FSE) T1-weighted sequence, as described by Sasaki et al.[76], with TR=600, TE=12, flip angle 111°, two echo trains. 13 slices (2.5 mm and 0.3-mm gaps) were acquired, with field of view 220 x 165 mm and matrix size 512 × 384. Three acquisitions were performed.

In both acquisition types, slices were acquired perpendicularly to the posterior aspect of fourth ventricle.

MRI data processing

Diffusion MRI

Diffusion MRI data were processed using Functional MRI of the Brain (FMRIB) Software Library (FSL, https://fsl.fmrib.ox.ac.uk/fsl/fslwiki). The "topup" program was used to estimate and correct susceptibility-induced off-resonance field using the two b=0 s/mm^2 images with opposite phase encoding.[77,78] The eddy "package" was then used to correct images for eddy current distortion, movement, and motion induced signal dropout.[79] The

Accelerated Microstructure Imaging via Convex Optimization (AMICO) package (https://github.com/daducci/AMICO) was used to fit the neurite orientation dispersion and density imaging (NODDI) model to the diffusion MRI data.[80]

A voxel-based analysis approach was used to register the diffusion images from all participants to a study specific template with the DTI-TK software (http://dti-tk.sourceforge.net/pmwiki/pmwiki.php).[81] The diffusion parameter images from NODDI along with the structural scans were all transformed into the template space. Regions of interest were drawn on the template and mean values of neurite density index (NDI), orientation dispersion index (ODI) and free water fraction (FWF or ISOvf) were extracted from each region. Regions of interest (ROIs) were placed bilaterally in the basal ganglia (anterior and posterior substantia nigra, putamen, pallidum, caudate) and in the pontine-cerebellar region (ventral pons, middle cerebellar peduncles, cerebellar white matter, and cortical cerebellar grey matter of lobule VI). ROIs covered (unilaterally) 168 voxels for the putamen, 22 voxels for the caudate, 72 voxels for the pallidum, 8 voxels for the anterior SN and 8 voxels for the posterior SN; all other ROIs covered 64 voxels. Two control regions were put on the occipital and parietal cortices. Anterior and posterior substantia nigra ROIs were placed after co-registering the diffusion MRI template to a template obtained from the magnetisation-transfer prepared GRE (neuromelanin-sensitive) scans, showing hyperintensity in the substantia nigra. This procedure ensured correct placement of SN ROIs while avoiding highly anisotropic cortico-spinal tracts. ROIs are shown in **Figure 2**.

Neuromelanin MRI

SN neuromelanin content was evaluated as follows. The two acquired MT GRE images of each participant were co-registered with SPM (https://www.fil.ion.ucl.ac.uk/spm/).

Neuromelanin content was estimated following Schwarz et al.[64] In brief, this methods estimates a hyperintense volume in the SN region exceeding a predefined background threshold, corresponding to voxels containing neuromelanin. Regions were manually drawn using ITK-SNAP (http://www.itksnap.org/)[82] on 3 consecutive slices best displaying the hyperintensity typical of substantia nigra in MT GRE scans. ROIs were drawn to cover anterior and posterior SN, cerebral peduncles and the central midbrain area. Using FSLUTILS in FSL, the mean and standard deviation (SD) of the intensity in the cerebral peduncles was determined, and then the volume of voxels in the SN exceeding the mean+3.25 SD intensity was calculated. The total volume of voxels containing neuromelanin was calculated for the anterior and posterior parts of the SN bilaterally.

LC neuromelanin content was evaluated as follows. The three FSE T1-weighted images of each participant were also co-registered and averaged. A slice-to-slice correction for intensity variation was performed so that each slice would match the brain mean intensity. This procedure was necessary to correct for intensity inhomogeneities in contiguous slices without compromising LC neuromelanin-associated hyperintensity. LC neuromelanin content was calculated following the method described in Doppler et al.[83] In brief, a "search ROI" was drawn on a MNI template following the LC coordinates described in Keren et al.[84] In order to investigate subregional LC differences, the search ROI was also divided with two axial planes in three parts: rostral, intermediate and caudal. A background volume of interest was centred in the pons matching the extension of the LC search ROIs. The MNI LC "search ROIs" were transformed to the individual FSE images for each subject using combined inverse transformations from MNI atlas space to anatomical T1 (derived from spatial normalisation of each subject's T1 image to MNI space) and from anatomical T1 to the FSE image (derived from a rigid transformation of the FSE to the T1 image). This allowed to estimate LC neuromelanin-associated hyperintensity in native space. Then, the 12 brightest

connected voxels in the entire LC "search ROI" and the five brightest connected voxels in each rostro-caudal subsection were identified. This procedure was carried out with a custom MATLAB (MathWorks, Natick, MS, USA) script employing SPM functions. The LC neuromelanin specific signal intensity for the entire LC and for each subsection was calculated as follows:

$$LC\ MRI\ contrast = \frac{mean\ ROI\ intensity - mean\ background\ ROI\ intensity}{mean\ background\ ROI\ intensity}$$

For the entire LC the mean intensity was derived from 12 brightest connected voxels. For each LC subdivision (rostral, intermediate, caudal) the mean intensity was derived from the 5 brightest connected voxels.

Statistical analysis

Median, interquartile range and values' range were used to describe demographics and general clinical characteristics. Given the relatively small number of patients present in each subgroup and the non-normal distribution of some clinical and neuroimaging measures, non-parametric tests were employed to carry out significance testing. Mann-Whitney U test was used to test differences in a variable between two independent groups (e.g. diffusion measures in PD and MSA patients). Kruskal-Wallis H test was used to test differences between two or more groups (e.g. neuromelanin content and diffusion measures between PD, MSA and controls); in this instance Dunn's test with Bonferroni correction was used for post-hoc significance testing. Associations between two variables were assessed with Spearman's rho correlation (e.g. association between LC integrity and MoCA scores).

Given the relatively small number of cases, especially in the MSA group, significance testing was restricted at independent-groups comparisons and correlations with potential biological meaning. As an example, comparisons were targeted at diffusion metrics in brain locations

known to be pathologically more affected in MSA patients, such as the putamen and the middle cerebellar peduncle. The same approach was used for correlations, e.g. in studying the association between LC, SN and cognitive scores. Given the exploratory nature of the NODDI and neuromelanin measures studied, and the restriction of multiple testing for each statistical test on a given set of variables in the same subset of subjects, p-values adjustment (e.g. family-wise error rate or false discovery rate) was not applied. This caveat will be considered in the interpretation of the results and analysed in the "Discussion" section.

Significance testing was two-tailed and the threshold for statistical significance was < 0.05. Statistical analyses were carried out with IBM Statistical Package for the Social Sciences (SPSS) Statistics version 27.

Results

Demographics and general clinical characteristics are shown in **Table 2**. No significant age or sex differences were present between the three groups.

Neuroimaging findings

Neuroimaging analysis was based on a region of interest (ROI) analysis.

Substantia nigra

PD and MSA showed significantly reduced neuromelanin content and increased free water fraction in the posterior (SN) compared to healthy controls (HC) (Kruskal-Wallis $H = 11.363$ $p = 0.003$ and $H = 8.784$, $p = 0.013$, respectively); neuromelanin content was also reduced in anterior SN ($H = 8.784$, $p = 0.013$). However, no significant differences could be identified between PD and MSA patients. No differences between patients and controls were identified in SN neurite density index (NDI) and orientation dispersion index (ODI). A trend for increased NDI in the posterior SN was present in PD and MSA patients ($H = 5.314$, $p = 0.070$) (**Table 3**). Interestingly, the average SN NDI of the substantia nigra, indicative of the intraneurite fraction, showed a direct association with free water fraction and an inverse association with neuromelanin content (**Figure 3**).

Diffusion metrics in extranigral locations

Diffusion metrics in extranigral locations were compared between MSA and PD patients, since these two entities represent the most compelling clinical diagnostic challenge. Differences in orientation dispersion index (ODI) and free water fraction (FWF, or isotropic

volume fraction) were investigated in grey matter ROIs, while differences in neurite dispersion index (NDI) were restricted to white matter ROIs. This approach was followed to restrict multiple comparisons to a minimum. The rationale for testing FWF and ODI in grey matter locations and NDI in white matter locations was based on the theoretical framework of what these parameters should represent in neuronal tissue, and on one previous NODDI study in parkinsonism.[52] Significantly increased free water fraction (FWF), indicative of neuronal loss, were identified in the putamen, caudate and cortical cerebellar grey matter of MSA patients compared to PD. Additionally, a non-significant trend for an increase of the orientation dispersion index (ODI) was present in the putamen and cerebellar grey matter of lobule VI in MSA. Significantly decreased neurite density index (NDI) in white matter locations, indicative of axonal loss, were identified in the MCP and ventral pons (**Table 4**).

Locus coeruleus neuromelanin

The MRI contrast of the entire LC, indicative of its neuromelanin content, was significantly reduced in MSA patients compared to HC ($H = 6.996$, $p = 0.030$; pairwise comparison MSA vs HC: Bonferroni adjusted $p = 0.026$). No significant differences between PD and HC or between PD and MSA were observed. Although the mean LC signal was lower in MSA than HC and PD patients in all LC subregions, significant differences were shown only in the intermediate portion ($H = 13.788$, $p = 0.001$; pairwise comparisons showing Bonferroni corrected p-values: PD vs HC $p = 0.039$; MSA vs HC = 0.001, PD vs MSA $p = 0.477$). No significant differences were present in the rostral and caudal subregions. **Figure 4** illustrates the distribution of LC MRI contrast in MSA, PD and HC.

Clinical correlates of neuroimaging findings

Motor symptoms

No significant correlations were identified between clinical severity in MSA patients as measured with UMSARS-I and UMSARS-II and microstructural abnormalities in the basal ganglia or in the ponto-cerebellar region.

Non-motor symptoms

Based on previous studies on the pathophysiology of specific non-motor symptoms in PD, we analysed whether depression, cognitive, RBD and dysautonomic scales scores were associated with degeneration in specific brain regions in the entire cohort of PD and MSA, and separately in MSA.

In the combined cohort of MSA and PD patients, depressive symptoms scores measured with the HADS-D scale were associated with increased caudate free water fraction (indicative of grey matter degeneration) (rho = 0.521, p = 0.004) and with locus coeruleus neuromelanin loss (entire LC: rho = -0.400, p=0.035; rostral LC: rho = -0.526, p=0.004; intermediate LC: rho = -0.389, p = 0.041; caudal LC: rho = 0.003, p = 0.988). No association was found between depression scores and SN microstructural abnormalities indices. In MSA patients, only the rostral LC remained significantly associated with depression scores (rho = -0.664, p = 0.026).

In the combined MSA and PD group, MoCA scores, reflecting general cognitive performances, were associated with neuromelanin content of the anterior SN (rho = 0.381, p = 0.041), but not of the posterior SN, and with rostral and intermediate LC subregions (rostral LC: rho = 0.470, p = 0.010; intermediate LC: rho = 0.554, p = 0.002). In MSA patients, only the association between rostral LC neuromelanin and MoCA scores remained significant (rho

= 0.770, p = 0.006; intermediate LC: rho = 0.567, p = 0.069). The relationship between MoCA scores, rostral LC and anterior SN is depicted in **Figure 5**.

RBDSQ scores, reflecting reported symptoms of REM sleep behaviour disorder, were not associated with LC neuromelanin content in the whole PD-MSA group. In MSA patients, RBD symptoms showed moderate inverse correlations with rostral and intermediate LC neuromelanin content (rho = -0.606, p = 0.048, rho = -0.592, p = 0.055, respectively), but not with the entire or caudal LC signal. Thus, greater neuromelanin loss in the rostral and intermediate parts of the LC are associated with more severe manifestations of RBD symptoms in MSA patients. Conversely, no associations were present between LC neuromelanin content and SCOPA sleep, a general scale that assesses mostly nocturnal insomnia and diurnal excessive daytime sleepiness. **Table 5** shows the relationship between LC subportions neuromelanin content and non-motor symptoms.

Since MoCA, HADS-D and RBDSQ scores correlated significantly with LC neuromelanin content, a correlation between these scores could be hypothesised. However, no significant correlations were found.

SCOPA-AUT scores, representing severity of autonomic symptoms, were not associated with diffusion measures in the cerebellar and basal ganglia regions, nor with neuromelanin content of LC and SN regions.

Discussion

In this study, a multimodal MRI approach, including diffusion MRI and neuromelanin-sensitive MRI, was used to investigate microstructural brain changes in the early stages of MSA and their association with motor and non-motor symptoms. One cohort of HC and one of established PD patients were also included.

The main findings may be summarised as follows. Neuromelanin and NODDI parameters in the SN and LC neuromelanin of MSA patients are significantly altered compared to healthy controls but are similar to PD patients. In extranigral grey matter locations, significant increases in free water fraction, indicative of more profound grey matter degeneration, were found in the putamen, caudate and cortical cerebellar grey matter in MSA compared to PD. In the putamen of MSA patients, the orientation dispersion index (ODI) was also decreased compared to PD, indicating alterations of the spatial organization of neurites, such as dendritic thinning.[22] In MSA, severity of cognitive, depressive and RBD symptoms were associated with LC neuromelanin loss, while motor and autonomic symptoms were not associated with NODDI and neuromelanin parameters.

These findings will be discussed in the following subsections.

Substantia nigra

Similarities in neurodegeneration as measured with dMRI and neuromelanin-sensitive MRI in the SN of PD and MSA patients are not surprising. Neuromelanin content was shown to be reduced similarly in the SN of PD and MSA patients in several studies.[66–69] This is also in keeping with similar striatal DaT availability in both conditions.[85] Recent evidence showed that greater SN neuromelanin content is associated with greater striatal dopamine release capacity as measured with ^{11}C-raclopride PET, [62] a D2/D3 receptor ligand. This seems to

point towards a rationale for using neuromelanin-sensitive MRI as a proxy measure of nigrostriatal dopaminergic function. Assessment of SN microstructural abnormalities with NODDI in MSA has been carried out by only two studies to date, both in patients with MSA-P.[52,86] Our cohort was predominantly composed of MSA-P patients but MSA-C were also included. Both studies identified increases in free water fraction and NDI in the SN of PD and MSA-P patients. While increases in free water can be interpreted with the increased presence of freely diffusing water, possibly due to atrophy and neuroinflammation, the increase in NDI has a non-trivial interpretation. Indeed, NDI (also referred to as intraneurite volume fraction) is a measure that corresponds to the water fraction with restricted diffusivity inside neurites and is calculated as a ratio between intraneurite and extraneurite water fractions.[22] Since extraneurite water fraction represents hindered water diffusivity typical of cell bodies (neurons' soma and glia), vasculature and extracellular matrices, a reduction of these, especially neuron cell bodies, could be responsible for this parameter's abnormality. Other cellular and tissue structural reorganization cannot be excluded. However, since pathological correlates of these MRI alterations are lacking, the interpretation of the specific tissue alteration in vivo is largely speculative. Interestingly, this parameter shows a direct association with free water fraction (greater values indicative of greater degeneration) and, most importantly, and inverse association with neuromelanin content (lower values indicative of greater dopaminergic neuron loss). Since the latter parameter is derived from a separate scanning sequence, it is tempting to think that progressive loss of neuromelanin in the SN is paralleled by tissue-level alterations that are captured by the NDI parameter yielded by NODDI. Pathological correlates of NODDI alterations are needed to elucidate these aspects, as well as further investigation on their sensitivity to longitudinal progression.

Locus coeruleus

In this study, LC neuromelanin content was found to be similarly reduced in PD and MSA compared to controls. This finding is corroborated by previous pathological evidence showing LC degeneration[87–90] and by a few previous neuroimaging studies investigating MSA patients with neuromelanin-sensitive MRI[67–69] or ^{18}F-DOPA PET.[91] Compared to those MRI studies, a different and possibly more detailed approach was taken here. First, the hyperintense signal of the locus coeruleus in the specific sequence was extracted in an automated fashion after delineating a "search ROI" on a standard template following previously described LC coordinates in MNI space.[84] This ensured that the maximum signal intensity was extracted from the correct location for each patient. Second, the search ROI was subdivided in three equal portions rostro-caudally to investigate subregional characteristics. Recently, Doppler et al. showed that the middle portion of the LC may be the most compromised LC location in PD compared to controls.[83] Subregional degeneration patterns of the LC have been shown pathologically, with greater degeneration in the caudal sections in PD and greater degeneration of the rostral sections in Alzheimer's Disease (AD).[92] The results of this study show that MSA patients in the early stages of the disease have a degree and subregional pattern of LC degeneration similar to PD. Significant differences compared to controls could only be identified in the intermediate section of the LC, possibly due to the small sample sizes of each cohort. In Doppler et al., the mean contrast of the caudal LC in PD patients was only slightly reduced, while differences were more evident in the middle portion.[83]

The branched projections of the LC reach almost all central nervous system locations: neocortex, hippocampus, amygdala, thalamus, cerebellum (reviewed extensively by Berridge and Waterhouse[93]).[94–96] In physiological conditions, LC noradrenaline release modulates cognition processes such as attention, learning memory and perception[97–100], but also stress responses, pain and autonomic functions.[101,102] Therefore, LC degeneration and its

subregional pattern might influence clinical manifestations such as cognitive functioning. It has been shown that post-mortem LC integrity is associated with late-life attenuation of cognitive decline, even when adjusting for other neurochemical systems integrity and comorbid pathology.[103] Another study used in vivo neuromelanin MRI to show that better memory performances in healthy young and older adults are associated with rostral LC integrity.[71] Thus, the association between MoCA scores and rostral LC neuromelanin found in MSA in this study adds to previous evidence in healthy subjects and AD patients.[71,104] The lack of association in PD patients may be due to the small sample size and a related small dispersion of MoCA values, a less strong association in this group, or both. It is interesting to note that in PD a moderate correlation (Spearman's rho = 0.394) between intermediate LC, where the greatest LC neuromelanin reduction is found, and MoCA scores exist. It is also worth noting that the MoCA is a general screening tool for cognitive impairment and therefore no clear association can be established with cognitive subdomains. Two recent studies in PD have shown an association between overall LC neuromelanin content and several cognitive subdomains, such as attention, executive functions, spatial orientation and verbal learning.[65,72] The authors hypothesize that this wide range of associations may be due to the widespread nature of the LC cortical projections and their degeneration in PD. To interpret these findings, it is also worth mentioning that Doppler et al. showed that noradrenergic terminal loss in remote locations exceeds on average 10-20% LC neuromelanin loss and the two measures are not correlated at the group level.[83]

A recent study by Prasuhn et al. showed moderate correlations in 45 PD patients between both SN and LC neuromelanin and Beck Depression Inventory (BDI) scale scores in PD.[65] In the current study, HADS-D scores, representing depressive symptoms, were significantly associated rostral LC neuromelanin loss in MSA only. This association is not surprising, given that LC dysfunction has been linked with depressive symptoms in major depression in

pathological[105], preclinical[106] and in vivo neuroimaging studies.[107,108] In light of the study by Prasuhn et al., non-significant associations in our PD group are probably due to its small sample size. It must also be acknowledged that in PD other determinants of depressive symptoms, such as striatal dopaminergic denervation[109] and cortical cholinergic denervation[110], should be considered. While striatal dopaminergic denervation is thought to drive depressive symptoms in PD[109], this pathophysiological link in MSA can only be speculative due to a lack of evidence. One study found acute levodopa administration ineffective in improving blunted affect characterizing MSA-P patients; the authors hypothesised that this trait could be due to caudate and ventral striatum degeneration and subsequent dysfunction of their connections with the orbitofrontal and limbic circuits.[111] In a ^{18}FDG-PET study, MSA depressive symptoms have been linked to reduced prefrontal metabolism[112], although this provides little information about the underlying neurochemical basis. Further studies on the neurochemical determinants of depression in MSA should be conducted as these would enable targeted pharmacological approaches.

In MSA patients, rostral LC neuromelanin loss also showed a significant association with RBD symptoms measured through the RBDSQ. The LC is thought to be part of a complex circuit responsible for the generation of REM sleep. However, the exact REM sleep generator nucleus in humans is still unclear and thought to reside in a group of neurons just rostral of the LC. These neurons are thought to be the analogous in humans of the peri-locus coeruleus alpha nucleus (or "subcoeruleus") in cat and sublaterodorsal nucleus in rat, and are glutammatergic.[113–115] Some naming confusion arises from the fact that in primates and human studies, the "subcoeruleus" is a caudal extension of the LC containing noradrenergic cells; the entire group is usually referred to as coeruleus-subcoeruleus complex.[116–118] It should be noted that in humans the REM sleep generator is also thought to be glutamatergic and to lie *rostrally* to the LC.[114] In previous studies, LC signal intensity has been shown to

correlate with the amount of REM sleep without atonia in a combined group of RBD patients and healthy controls[119], and to be reduced in PD patients with RBD compared to those without RBD.[120,121] In patients with RBD, greater REM sleep without atonia was correlated with greater LC neuromelanin loss[121], although this finding was not confirmed by others.[120] In this study, RBDSQ was not correlated with LC signal intensity in PD. However, it should be considered that no selection was made in terms of RBD symptoms. The moderate-strong correlation found between RBDSQ and rostral LC signal intensity in MSA could be caused by a greater contribution of LC dysfunction to RBD generation in MSA compared to PD (in which other mechanisms such as pedunculopontine cholinergic dysfunction may also contribute), but also by a greater severity of pathology in pontine neighbouring structures controlling REM sleep. In either case, LC degeneration as measured by neuromelanin-sensitive MRI in MSA could provide pathophysiological information regarding RBD symptoms and be used as a proxy measure of damage to adjacent tegmental pontine structures.

No associations were found between LC neuromelanin loss and severity of autonomic symptoms as measured by SCOPA-AUT scores. One study showed lower ^{18}F-DOPA uptake in the LC in MSA patients with orthostatic hypotension compared to those without.[91] Since LC is thought to be implicated in central autonomic regulation of cardiovascular function[102,122], a more clinically detailed approach could uncover meaningful associations.

Finally, the overall topography of LC degeneration and its association with scales scores should be discussed. Indeed, the MRI contrast is greatest in the LC rostral section and decreases caudally. This implies that differences between subgroups and associations with clinical scores may be more detectable rostrally. Therefore, the pattern of LC degeneration seen in both PD and MSA, with variable rostral neuromelanin reductions and more consistent reductions in the intermediate part, seem to reflect pathological reports describing a caudo-

rostral gradient of degeneration. The lack of significant differences in the most caudal part may be due insufficient signal-to-noise ratio (SNR). In MSA, moderate or strong correlation coefficients between rostral and intermediate LC and scales scores of cognitive impairment, depression and RBD symptoms were found. These could be indicative of a true pathophysiological link with rostral LC dysfunction, or could be partly due to a better SNR in this section. In the latter case, the association would not be invalidated, rather this would imply that the group distribution of rostral LC degeneration severity would serve as a proxy for the entire LC, given the profound signal loss in the more caudal parts.

Diffusion MRI parameters in extranigral locations

Diffusion MRI parameters have been used to investigate typical pathological alterations in white and grey matter in MSA, with most studies using the DTI model.[25–27,32,37,123,124] More recently, automatized image processing and data classification algorithms have shown that multiple parameters from multiple locations may be useful in distinguishing PD and MSA (and atypical parkinsonism in general) with good accuracy.[52–54,125] In the current study, NODDI was used to study critical brain locations in MSA and PD. Compared to PD, MSA patients showed increased free water fraction, indicative of grey matter loss, in putamen, caudate and cerebellar grey matter of lobule VI. Reductions in NDI were identified in the MCP and ventral pons ($p=0.50$), indicative of white matter degeneration. NODDI application in MSA could be particularly valuable since it simultaneously provides meaningful multiple information about grey and white matter structure. Only two recent studies have applied NODDI in parkinsonism, both in MSA-P patients.[52,86] The NODDI parameters found in nigral and extranigral locations in the present study parallel those found in such studies, likely indicating high repeatability of this technique across studies and sites.

Limitations of the study

Some limitations should be addressed. Although MSA is a rare condition, the number of MSA patients included in this study is rather small. Therefore, results should be interpreted with caution. However, findings from both NODDI and neuromelanin MRI and their associations with clinical scores seem to reflect and expand previous knowledge and retain pathophysiological significance, as discussed in the previous paragraphs. It is likely that larger studies will provide a greater degree of certainty.

Given the low number of patients included in the study, hypothesis testing was limited and targeted to test a priori plausible differences and associations. Therefore, some unexpected but meaningful results could have been missed. Furthermore, a p-value correction for multiple testing was not applied. This decision was driven by the exploratory nature of this study and the small number of MSA patients included, as statistical power could have been hampered. The lack of correction for multiple tests could have inflated the type I error (i.e. a number of falsely significant results may have been reported). However, at $p < 0.05$ the probability of a false positive is one in 20, meaning that every 20 statistical tests conducted, one will be falsely significant. The overall number of statistical tests involving significance testing carried out in this study was kept to a minimum and should have produced less than five false positives. Keeping this in mind, the overall interpretation of the results will not change. Rather, this reinstates the need to interpret results with caution, especially where small effects were reported.

The lack of detailed neuropsychological assessments, a more detailed assessment of depressive symptoms and polysomnography represent intrinsic limitations of this study. Since this was primarily a neuroimaging analysis, the decision to rapidly screen for more

symptoms prevailed over the detailed assessment of only one or two symptoms, which would have needed far greater time, resources and patients' compliance.

Future directions and other biomarkers

Neuroimaging biomarkers now provide optimal diagnostic accuracy for MSA and PD, although their implementation in clinical practice is largely incomplete. The next major goal will be to achieve the earliest possible diagnosis in order to provide the possibility of early symptomatic treatment and the inclusion of these patients in clinical trials. Neuroimaging biomarkers also provide important information about the pathophysiological mechanisms of symptoms. This information may be used to target specific dysfunctions with pharmacological and non-pharmacological approaches.

In recent years, fluid biomarkers derived from cerebrospinal fluid (CSF) and plasma have also provided a great amount of information about the CNS ongoing pathological process. Plasma norepinephrine levels have been shown to be a promising tool in distinguishing MSA from PD. In MSA, autonomic dysfunction is due to the degeneration of the central autonomic nuclei, while in PD it is due to degeneration of autonomic nerve fibres in the peripheral nervous system (PNS). Elevated levels of plasma NE have also been shown in patients with prodromal autonomic dysfunction who later converted to MSA.[126,127] One CSF and plasma marker of neuronal injury, neurofilament light chain (NFL) is elevated in atypical parkinsonism compared to PD.[128,129] In a meta-analysis of 8 studies, the pooled sensitivity in differentiating MSA from PD was 82% (95% confidence interval, CI: 71%–93%) and specificity was 87% (95% CI: 80%–90%).[130] Another marker of neuronal injury, the total and phosphorylated tau protein, does not show differences in MSA compared to PD and HC, although a higher total tau / beta amyloid 42 ($A\beta_{42}$) ratio in MSA compared to PD was shown

to have acceptable sensitivity and specificity in differentiating the two conditions (78.6% sensitivity, 80% specificity).[131] Finally, CSF alpha-synuclein levels are similarly reduced in PD and MSA compared to controls[132], but more recent techniques may exploit different molecular characteristics of alpha-synuclein in these conditions. Protein misfolding cyclic amplification (PMCA) and real-time quacking-induced conversion (RT QuIC) are protein aggregation assays that can be used to amplify and detect alpha-synuclein oligomers, soluble misfolded aggregates that can be found in CSF.[133,134] In MSA these assays have shown different biochemical and biophysical characteristics compared to PD, due to molecular structural differences[134], that allow very high discrimination between MSA, PD and controls.[135–137]

Overall, it is possible that in the near future a combination of biomarkers from different sources (e.g. neuroimaging, CSF, plasma) may be available to assist the clinical diagnosis, to formulate prognostic predictions and to observe disease-modifying effects in clinical trials.

Conclusion

In this study, a detailed neuroimaging analysis including NODDI, a novel diffusion MRI technique, and neuromelanin were carried out in early stage MSA and compared to PD patients and healthy controls. MSA patients showed neuromelanin reductions and diffusion parameter alterations in SN and LC similar to PD, but greater degeneration in the putamen, caudate, cerebellar cortex and MCP. These in vivo findings closely resemble known pathological findings and could be used in the future as diagnostic and progression biomarkers. Furthermore, it was shown that LC degeneration seems a strong driver, even more than in PD, of cognitive impairment, depressive symptoms and RBD symptoms. These

associations should be further explored to identify new possible treatment approaches, largely lacking in MSA.

References

1. Gilman S, Wenning GK, Low PA, et al. Second consensus statement on the diagnosis of multiple system atrophy. *Neurology*. 2008;71(9):670-676. doi:10.1212/01.WNL.0000324625.00404.15

2. Papp MI, Kahn JE, Lantos PL. Glial cytoplasmic inclusions in the CNS of patients with multiple system atrophy (striatonigral degeneration, olivopontocerebellar atrophy and Shy-Drager syndrome). *J Neurol Sci*. 1989;94(1-3):79-100. doi:10.1016/0022-510X(89)90219-0

3. Tu P, Galvin JE, Baba M, et al. Glial cytoplasmic inclusions in white matter oligodendrocytes of multiple system atrophy brains contain insoluble α-synuclein. *Ann Neurol*. 1998;44(3):415-422. doi:10.1002/ANA.410440324

4. Ozawa T, Paviour D, Quinn NP, et al. The spectrum of pathological involvement of the striatonigral and olivopontocerebellar systems in multiple system atrophy: clinicopathological correlations. *Brain*. 2004;127(12):2657-2671. doi:10.1093/BRAIN/AWH303

5. Trojanowski JQ, Revesz T. Proposed neuropathological criteria for the post mortem diagnosis of multiple system atrophy. *Neuropathol Appl Neurobiol*. 2007;33(6):615-620. doi:10.1111/J.1365-2990.2007.00907.X

6. Papp MI, Lantos PL. The distribution of oligodendroglial inclusions in multiple system atrophy and its relevance to clinical symptomatology. *Brain*. 1994;117:235-243. https://academic.oup.com/brain/article/117/2/235/290574. Accessed September 17, 2021.

7. Jellinger KA. Neuropathology of multiple system atrophy: New thoughts about pathogenesis. *Mov Disord*. 2014;29(14):1720-1741. doi:10.1002/mds.26052

8. Wenning GK, Tison F, Shlomo Y ben, Daniel SE, Quinn NP. Multiple system atrophy: A review of 203 pathologically proven cases. *Mov Disord*. 1997;12(2):133-147. doi:10.1002/MDS.870120203

9. Cykowski MD, Coon EA, Powell SZ, et al. Expanding the spectrum of neuronal pathology in multiple system atrophy. *Brain*. 2015;138(8):2293-2309. doi:10.1093/BRAIN/AWV114

10. Jellinger KA. Neuropathology of sporadic Parkinson's disease: Evaluation and changes of concepts. *Mov Disord*. 2012;27(1):8-30. doi:10.1002/MDS.23795

11. O'Sullivan SS, Massey LA, Williams DR, et al. Clinical outcomes of progressive supranuclear palsy and multiple system atrophy. *Brain*. 2008;131(5):1362-1372. doi:10.1093/BRAIN/AWN065

12. Wenning GK, Geser F, Krismer F, et al. The natural history of multiple system atrophy: a prospective European cohort study. *Lancet Neurol*. 2013;12(3):264-274. doi:10.1016/S1474-4422(12)70327-7

13. Coon EA, Ahlskog JE. My Treatment Approach to Multiple System Atrophy. *Mayo Clin Proc*. 2021;96(3):708-719. doi:10.1016/J.MAYOCP.2020.10.005

14. Mori S, Barker PB. Diffusion magnetic resonance imaging: Its principle and applications. *Anat Rec*. 1999;257(3):102-109. doi:10.1002/(SICI)1097-0185(19990615)257:3<102::AID-AR7>3.0.CO;2-6

15. Pierpaoli C, Jezzard P, Basser PJ, Barnett A, Di Chiro G. Diffusion tensor MR imaging of the human brain. *Radiology*. 1996;201(3):637-648. doi:10.1148/radiology.201.3.8939209

16. Basser PJ, Mattiello J, Lebihan D. Estimation of the Effective Self-Diffusion Tensor from the NMR Spin Echo. *J Magn Reson Ser B*. 1994;103(3):247-254.

doi:10.1006/JMRB.1994.1037

17. Soares JM, Marques P, Alves V, Sousa N. A hitchhiker's guide to diffusion tensor imaging. *Front Neurosci*. 2013;7(7 MAR):1-14. doi:10.3389/fnins.2013.00031

18. Wilde EA, Ayoub KW, Choudhri AF. *Diffusion Tensor Imaging*. Vol 1. (Papanicolaou AC, ed.). Oxford University Press; 2014. doi:10.1093/oxfordhb/9780199764228.013.10

19. Smith SM, Jenkinson M, Johansen-Berg H, et al. Tract-based spatial statistics: Voxelwise analysis of multi-subject diffusion data. *Neuroimage*. 2006;31(4):1487-1505. doi:10.1016/j.neuroimage.2006.02.024

20. Pasternak O, Sochen N, Gur Y, Intrator N, Assaf Y. Free water elimination and mapping from diffusion MRI. *Magn Reson Med*. 2009;62(3):717-730. doi:10.1002/mrm.22055

21. Jensen JH, Helpern JA. MRI quantification of non-Gaussian water diffusion by kurtosis analysis. *NMR Biomed*. 2010;23(7):698-710. doi:10.1002/nbm.1518

22. Zhang H, Schneider T, Wheeler-Kingshott CA, Alexander DC. NODDI: Practical in vivo neurite orientation dispersion and density imaging of the human brain. *Neuroimage*. 2012;61(4):1000-1016. doi:10.1016/j.neuroimage.2012.03.072

23. Kamiya K, Hori M, Aoki S. NODDI in clinical research. *J Neurosci Methods*. 2020;346:108908. doi:10.1016/J.JNEUMETH.2020.108908

24. Seppi K, Schocke MFH, Esterhammer R, et al. Diffusion-weighted imaging discriminates progressive supranuclear palsy from PD, but not from the parkinson variant of multiple system atrophy. *Neurology*. 2003;60(6):922-927. doi:10.1212/01.WNL.0000049911.91657.9D

25. Schocke MFH, Seppi K, Esterhammer R, et al. Diffusion-weighted MRI differentiates the Parkinson variant of multiple system atrophy from PD. *Neurology*. 2002;58(4):575-580. doi:10.1212/WNL.58.4.575

26. Nicoletti G, Lodi R, Condino F, et al. Apparent diffusion coefficient measurements of the middle cerebellar peduncle differentiate the Parkinson variant of MSA from Parkinson's disease and progressive supranuclear palsy. *Brain*. 2006;129(10):2679-2687. doi:10.1093/brain/awl166

27. Pellecchia MT, Barone P, Mollica C, et al. Diffusion-weighted imaging in multiple system atrophy: A comparison between clinical subtypes. *Mov Disord*. 2009;24(5):689-696. doi:10.1002/mds.22440

28. Ito M, Watanabe H, Atsuta N, et al. Fractional anisotropy values detect pyramidal tract involvement in multiple system atrophy. *J Neurol Sci*. 2008;271(1-2):40-46. doi:10.1016/j.jns.2008.03.013

29. Tir M, Delmaire C, le Thuc V, et al. Motor-related circuit dysfunction in MSA-P: Usefulness of combined whole-brain imaging analysis. *Mov Disord*. 2009;24(6):863-870. doi:10.1002/mds.22463

30. Cnyrim CD, Kupsch A, Ebersbach G, Hoffmann K-T. Diffusion Tensor Imaging in Idiopathic Parkinson's Disease and Multisystem Atrophy (Parkinsonian Type). *Neurodegener Dis*. 2013;13(1):1-8. doi:10.1159/000348512

31. Ji L, Zhu D, Xiao C, Shi J. Tract based spatial statistics in multiple system atrophy: A comparison between clinical subtypes. *Parkinsonism Relat Disord*. 2014;20(10):1050-1055. doi:10.1016/j.parkreldis.2014.06.017

32. Worker A, Blain C, Jarosz J, et al. Diffusion tensor imaging of Parkinson's disease, multiple system atrophy and progressive supranuclear palsy: A tract-based spatial

statistics study. *PLoS One*. 2014;9(11). doi:10.1371/journal.pone.0112638

33. Fukui Y, Hishikawa N, Sato K, et al. Characteristic diffusion tensor tractography in multiple system atrophy with predominant cerebellar ataxia and cortical cerebellar atrophy. *J Neurol*. 2016;263(1):61-67. doi:10.1007/s00415-015-7934-x

34. Del Campo N, Phillips O, Ory-Magne F, et al. Broad white matter impairment in multiple system atrophy. *Hum Brain Mapp*. 2021;42(2):357-366. doi:10.1002/hbm.25227

35. Faber J, Giordano I, Jiang X, et al. Prominent White Matter Involvement in Multiple System Atrophy of Cerebellar Type. *Mov Disord*. 2020;35(5):816-824. doi:10.1002/mds.27987

36. Baudrexel S, Seifried C, Penndorf B, et al. The value of putaminal diffusion imaging versus 18-fluorodeoxyglucose positron emission tomography for the differential diagnosis of the Parkinson variant of multiple system atrophy. *Mov Disord*. 2014;29(3):380-387. doi:10.1002/mds.25749

37. Barbagallo G, Sierra-Peña M, Nemmi F, et al. Multimodal MRI assessment of nigro-striatal pathway in multiple system atrophy and Parkinson disease. *Mov Disord*. 2016;31(3):325-334. doi:10.1002/mds.26471

38. Planetta PJ, Ofori E, Pasternak O, et al. Free-water imaging in Parkinson's disease and atypical parkinsonism. *Brain*. 2016;139(2):495-508. doi:10.1093/brain/awv361

39. Pasternak O, Westin C-F, Bouix S, et al. Excessive Extracellular Volume Reveals a Neurodegenerative Pattern in Schizophrenia Onset. *J Neurosci*. 2012;32(48):17365. doi:10.1523/JNEUROSCI.2904-12.2012

40. Burciu RG, Ofori E, Archer DB, et al. Progression marker of Parkinson's disease: A 4-year multi-site imaging study. *Brain*. 2017;140(8):2183-2192.

doi:10.1093/brain/awx146

41. Ofori E, Pasternak O, Planetta PJ, et al. Increased free-water in the substantia nigra of Parkinson's disease: a single-site and multi-site study. *Neurobiol Aging*. 2015;36(2):1097. doi:10.1016/J.NEUROBIOLAGING.2014.10.029

42. Seppi K, Schocke MFH, Donnemiller E, et al. Comparison of diffusion-weighted imaging and [123I]IBZM-SPECT for the differentiation of patients with the Parkinson variant of multiple system atrophy from those with Parkinson's disease. *Mov Disord*. 2004;19(12):1438-1445. doi:10.1002/mds.20229

43. Chung EJ, Kim EG, Bae JS, et al. Usefulness of Diffusion-Weighted MRI for Differentiation between Parkinson's Disease and Parkinson Variant of Multiple System Atrophy. *J Mov Disord*. 2009;2(2):64-68. doi:10.14802/jmd.09017

44. Kanazawa M, Shimohata T, Terajima K, et al. Quantitative evaluation of brainstem involvement in multiple system atrophy by diffusion-weighted MR imaging. *J Neurol*. 2004;251(9):1121-1124. doi:10.1007/s00415-004-0494-0

45. Paviour DC, Thornton JS, Lees AJ, Jäger HR. Diffusion-weighted magnetic resonance imaging differentiates parkinsonian variant of multiple-system atrophy from progressive supranuclear palsy. *Mov Disord*. 2007;22(1):68-74. doi:10.1002/mds.21204

46. Seppi K, Schocke MFH, Prennschuetz-Schuetzenau K, et al. Topography of putaminal degeneration in multiple system atrophy: A diffusion magnetic resonance study. *Mov Disord*. 2006;21(6):847-852. doi:10.1002/mds.20843

47. Köllensperger M, Seppi K, Liener C, et al. Diffusion weighted imaging best discriminates PD from MSA-P: A comparison with tilt table testing and heart MIBG scintigraphy. *Mov Disord*. 2007;22(12):1771-1776. doi:10.1002/mds.21614

48. A K, A T, Y H. Neuronal cell loss of the striatonigral system in multiple system atrophy. *J Neurol Sci*. 1993;117(1-2):33-40. doi:10.1016/0022-510X(93)90151-N

49. Seppi K, Schocke MFH, Mair KJ, et al. Progression of putaminal degeneration in multiple system atrophy: A serial diffusion MR study. *Neuroimage*. 2006;31(1):240-245. doi:10.1016/j.neuroimage.2005.12.006

50. Pellecchia MT, Barone P, Vicidomini C, et al. Progression of striatal and extrastriatal degeneration in multiple system atrophy: A longitudinal diffusion-weighted MR study. *Mov Disord*. 2011;26(7):1303-1309. doi:10.1002/mds.23601

51. Umemura A, Oeda T, Hayashi R, et al. Diagnostic Accuracy of Apparent Diffusion Coefficient and 123I-Metaiodobenzylguanidine for Differentiation of Multiple System Atrophy and Parkinson's Disease. *PLoS One*. 2013;8(4):1-7. doi:10.1371/journal.pone.0061066

52. Mitchell T, Archer DB, Chu WT, et al. Neurite orientation dispersion and density imaging (NODDI) and free-water imaging in Parkinsonism. *Hum Brain Mapp*. 2019;40(17):5094-5107. doi:10.1002/hbm.24760

53. Archer DB, Bricker JT, Chu WT, et al. Development and validation of the automated imaging differentiation in parkinsonism (AID-P): a multicentre machine learning study. *Lancet Digit Heal*. 2019;1(5):e222-e231. doi:10.1016/S2589-7500(19)30105-0

54. Krismer F, Beliveau V, Seppi K, et al. Automated Analysis of Diffusion-Weighted Magnetic Resonance Imaging for the Differential Diagnosis of Multiple System Atrophy from Parkinson's Disease. *Mov Disord*. 2021;36(1):241-245. doi:10.1002/mds.28281

55. Zecca L, Bellei C, Costi P, et al. New melanic pigments in the human brain that accumulate in aging and block environmental toxic metals. *Proc Natl Acad Sci*.

2008;105(45):17567-17572. doi:10.1073/PNAS.0808768105

56. Sulzer D, Zecca L. Intraneuronal dopamine-quinone synthesis: A review. *Neurotox Res 2000 13*. 1999;1(3):181-195. doi:10.1007/BF03033289

57. Zucca FA, Vanna R, Cupaioli FA, et al. Neuromelanin organelles are specialized autolysosomes that accumulate undegraded proteins and lipids in aging human brain and are likely involved in Parkinson's disease. *npj Park Dis 2018 41*. 2018;4(1):1-23. doi:10.1038/s41531-018-0050-8

58. Sasaki M, Shibata E, Tohyama K, et al. Neuromelanin magnetic resonance imaging of locus ceruleus and substantia nigra in Parkinson's disease. *Neuroreport*. 2006;17(11):1215-1218. doi:10.1097/01.wnr.0000227984.84927.a7

59. Trujillo P, Summers PE, Ferrari E, et al. Contrast mechanisms associated with neuromelanin-MRI. *Magn Reson Med*. 2017;78(5):1790-1800. doi:10.1002/MRM.26584

60. Langley J, Huddleston DE, Chen X, Sedlacik J, Zachariah N, Hu X. A multicontrast approach for comprehensive imaging of substantia nigra. *Neuroimage*. 2015;112:7-13. doi:10.1016/J.NEUROIMAGE.2015.02.045

61. Xing Y, Sapuan A, Dineen RA, Auer DP. Life span pigmentation changes of the substantia nigra detected by neuromelanin-sensitive MRI. *Mov Disord*. 2018;33(11):1792. doi:10.1002/MDS.27502

62. Cassidy CM, Zucca FA, Girgis RR, et al. Neuromelanin-sensitive MRI as a noninvasive proxy measure of dopamine function in the human brain. doi:10.1073/pnas.1807983116

63. Kraemmer J, Kovacs GG, Perju-Dumbrava L, Pirker S, Traub-Weidinger T, Pirker W. Correlation of striatal dopamine transporter imaging with post mortem substantia nigra

cell counts. *Mov Disord*. 2014;29(14):1767-1773. doi:10.1002/MDS.25975

64. Schwarz ST, Xing Y, Tomar P, Bajaj N, Auer DP. In Vivo Assessment of Brainstem Depigmentation in Parkinson Disease: Potential as a Severity Marker for Multicenter Studies. *Radiology*. 2017;283(3):789-798. doi:10.1148/RADIOL.2016160662

65. Prasuhn J, Prasuhn M, Fellbrich A, et al. Association of Locus Coeruleus and Substantia Nigra Pathology With Cognitive and Motor Functions in Patients With Parkinson Disease. *Neurology*. 2021;97(10):e1007-e1016. doi:10.1212/WNL.0000000000012444

66. Kashihara K, Shinya T, Higaki F. Reduction of neuromelanin-positive nigral volume in patients with MSA, PSP and CBD. *Intern Med*. 2011;50(16):1683-1687. doi:10.2169/internalmedicine.50.5101

67. Matsuura K, Maeda M, Yata K, et al. Neuromelanin magnetic resonance imaging in Parkinson's disease and multiple system atrophy. *Eur Neurol*. 2013;70(1-2):70-77. doi:10.1159/000350291

68. Ohtsuka C, Sasaki M, Konno K, et al. Differentiation of early-stage parkinsonisms using neuromelanin-sensitive magnetic resonance imaging. *Park Relat Disord*. 2014;20(7):755-760. doi:10.1016/j.parkreldis.2014.04.005

69. Matsuura K, Ii Y, Maeda M, et al. Neuromelanin-sensitive magnetic resonance imaging in disease differentiation for parkinsonism or neurodegenerative disease affecting the basal ganglia. *Park Relat Disord*. 2021;87(April):75-81. doi:10.1016/j.parkreldis.2021.05.002

70. Simões RM, Castro Caldas A, Grilo J, et al. A distinct neuromelanin magnetic resonance imaging pattern in parkinsonian multiple system atrophy. *BMC Neurol*. 2020;20(1):1-12. doi:10.1186/s12883-020-02007-5

71. Dahl MJ, Mather M, Düzel S, et al. Rostral locus coeruleus integrity is associated with better memory performance in older adults. *Nat Hum Behav*. 2019;3(11):1203-1214. doi:10.1038/s41562-019-0715-2

72. Li Y, Wang C, Wang J, et al. Mild cognitive impairment in de novo Parkinson's disease: A neuromelanin MRI study in locus coeruleus. *Mov Disord*. 2019;34(6):884-892. doi:10.1002/MDS.27682

73. Hughes AJ, Daniel SE, Kilford L, Lees AJ. Accuracy of clinical diagnosis of idiopathic Parkinson's disease: a clinico-pathological study of 100 cases. *J Neurol Neurosurg Psychiatry*. 1992;55(3):181-184. doi:10.1136/jnnp.55.3.181

74. van der Pluijm M, Cassidy C, Zandstra M, et al. Reliability and Reproducibility of Neuromelanin-Sensitive Imaging of the Substantia Nigra: A Comparison of Three Different Sequences. *J Magn Reson Imaging*. 2021;53(3):712-721. doi:10.1002/JMRI.27384

75. Langley J, Huddleston DE, Liu CJ, Hu X. Reproducibility of locus coeruleus and substantia nigra imaging with neuromelanin sensitive MRI. *Magn Reson Mater Physics, Biol Med*. 2017;30(2):121-125. doi:10.1007/S10334-016-0590-Z/FIGURES/3

76. Sasaki M, Shibata E, Kudo K, Tohyama K, Neuromelanin MRI al. Neuromelanin-Sensitive MRI Basics, Technique, and Clinical Applications Neuromelaninsensitive MRT. Grundlagen, Technik und klinische Einsatzmöglichkeiten Neuroradiology Clinical. *Clin Neuroradiol*. 2008;18(3):147-153. doi:10.1007/s00062-008-8018-4

77. Andersson JLR, Skare S, Ashburner J. How to correct susceptibility distortions in spin-echo echo-planar images: application to diffusion tensor imaging. *Neuroimage*. 2003;20(2):870-888. doi:10.1016/S1053-8119(03)00336-7

78. Smith SM, Jenkinson M, Woolrich MW, et al. Advances in functional and structural

MR image analysis and implementation as FSL. *Neuroimage*. 2004;23 Suppl 1(SUPPL. 1). doi:10.1016/J.NEUROIMAGE.2004.07.051

79. Andersson JLR, Sotiropoulos SN. An integrated approach to correction for off-resonance effects and subject movement in diffusion MR imaging. *Neuroimage*. 2016;125:1063-1078. doi:10.1016/J.NEUROIMAGE.2015.10.019

80. Daducci A, Canales-Rodríguez EJ, Zhang H, Dyrby TB, Alexander DC, Thiran JP. Accelerated Microstructure Imaging via Convex Optimization (AMICO) from diffusion MRI data. *Neuroimage*. 2015;105:32-44. doi:10.1016/J.NEUROIMAGE.2014.10.026

81. Zhang H, Yushkevich PA, Rueckert D, Gee JC. Unbiased white matter atlas construction using diffusion tensor images. *Med Image Comput Comput Assist Interv*. 2007;10(Pt 2):211-218. doi:10.1007/978-3-540-75759-7_26

82. Yushkevich PA, Piven J, Hazlett HC, et al. User-guided 3D active contour segmentation of anatomical structures: Significantly improved efficiency and reliability. *Neuroimage*. 2006;31(3):1116-1128. doi:10.1016/J.NEUROIMAGE.2006.01.015

83. Doppler CEJ, Kinnerup MB, Brune C, et al. Regional locus coeruleus degeneration is uncoupled from noradrenergic terminal loss in Parkinson's disease. *Brain*. 2021;144(9):2732-2744. doi:10.1093/BRAIN/AWAB236

84. Keren NI, Lozar CT, Harris KC, Morgan PS, Eckert MA. In vivo mapping of the human locus coeruleus. *Neuroimage*. 2009;47(4):1261-1267. doi:10.1016/j.neuroimage.2009.06.012

85. Pirker W, Asenbaum S, Bencsits G, et al. [123I]β-CIT spect in multiple system atrophy, progressive supranuclear palsy, and corticobasal degeneration. *Mov Disord*.

2000;15(6):1158-1167. doi:10.1002/1531-8257(200011)15:6<1158::AID-MDS1015>3.0.CO;2-0

86. Ogawa T, Hatano T, Kamagata K, et al. White matter and nigral alterations in multiple system atrophy-parkinsonian type. *NPJ Park Dis*. 2021;7(1):96. doi:10.1038/S41531-021-00236-0

87. Lüthy F, Mumenthaler M. Der Locus coeruleus bei der olivo-ponto-cerebellären Atrophie. *Arch für Psychiatr und Nervenkrankheiten 1958 1974*. 1958;197(4):327-334. doi:10.1007/BF00345841

88. Spokes EGS, Bannister R, Oppenheimer DR. Multiple system atrophy with autonomic failure. *J Neurol Sci*. 1979;43(1):59-82. doi:10.1016/0022-510X(79)90073-X

89. Tomonaga M. Neuropathology of the locus ceruleus: a semi-quantitative study. *J Neurol*. 1983;230(4):231-240. doi:10.1007/BF00313699

90. Berciano J, Valldeoriola F, Ferrer I, et al. Presynaptic parkinsonism in multiple system atrophy mimicking parkinson's disease: A clinicopathological case study. *Mov Disord*. 2002;17(4):812-816. doi:10.1002/mds.10190

91. Lewis SJ, Pavese N, Rivero-Bosch M, et al. Brain monoamine systems in multiple system atrophy: a positron emission tomography study. *Neurobiol Dis*. 2012;46(1):130-136. doi:10.1016/J.NBD.2011.12.053

92. German DC, Manaye KF, White CL, et al. Disease-specific patterns of locus coeruleus cell loss. *Ann Neurol*. 1992;32(5):667-676. doi:10.1002/ANA.410320510

93. Berridge CW, Waterhouse BD. The locus coeruleus–noradrenergic system: modulation of behavioral state and state-dependent cognitive processes. *Brain Res Rev*. 2003;42(1):33-84. doi:10.1016/S0165-0173(03)00143-7

94. Lindvall O, Bjorklund A. The organization of the ascending catecholamine neuron systems in the rat brain. As revealed by the glyoxylic acid fluorescence method. *Acta Physiol Scand*. 1974;92(sup. 412). https://www.unboundmedicine.com/medline/citation/4531814/The_organization_of_the_ascending_catecholamine_neuron_systems_in_the_rat_brain_as_revealed_by_the_glyoxylic_acid_fluorescence_method_. Accessed December 7, 2021.

95. Swanson LW, Hartman BK. The central adrenergic system. An immunofluorescence study of the location of cell bodies and their efferent connections in the rat utilizing dopamine-B-hydroxylase as a marker. *J Comp Neurol*. 1975;163(4):467-505. doi:10.1002/CNE.901630406/FORMAT/PDF

96. Jones BE, Halaris AE, McIlhany M, Moore RY. Ascending projections of the locus coeruleus in the rat. I. Axonal transport in central noradrenaline neurons. *Brain Res*. 1977;127(1):1-21. doi:10.1016/0006-8993(77)90377-8

97. Berridge CW, Waterhouse BD. The locus coeruleus-noradrenergic system: modulation of behavioral state and state-dependent cognitive processes. *Brain Res Brain Res Rev*. 2003;42(1):33-84. doi:10.1016/S0165-0173(03)00143-7

98. Arnsten AFT, Li BM. Neurobiology of executive functions: catecholamine influences on prefrontal cortical functions. *Biol Psychiatry*. 2005;57(11):1377-1384. doi:10.1016/J.BIOPSYCH.2004.08.019

99. Mather M, Clewett D, Sakaki M, Harley CW. Norepinephrine ignites local hotspots of neuronal excitation: How arousal amplifies selectivity in perception and memory. *Behav Brain Sci*. 2016;39. doi:10.1017/S0140525X15000667

100. Sara SJ. The locus coeruleus and noradrenergic modulation of cognition. *Nat Rev Neurosci*. 2009;10(3):211-223. doi:10.1038/NRN2573

101. Samuels ER, Szabadi E. Functional Neuroanatomy of the Noradrenergic Locus Coeruleus: Its Roles in the Regulation of Arousal and Autonomic Function Part II: Physiological and Pharmacological Manipulations and Pathological Alterations of Locus Coeruleus Activity in Humans. *Curr Neuropharmacol*. 2008;6(3):254. doi:10.2174/157015908785777193

102. Wang X, Piñol RA, Byrne P, Mendelowitz D. Optogenetic Stimulation of Locus Ceruleus Neurons Augments Inhibitory Transmission to Parasympathetic Cardiac Vagal Neurons via Activation of Brainstem α1 and β1 Receptors. *J Neurosci*. 2014;34(18):6182-6189. doi:10.1523/JNEUROSCI.5093-13.2014

103. Wilson RS, Nag S, Boyle PA, et al. Neural reserve, neuronal density in the locus ceruleus, and cognitive decline. *Neurology*. 2013;80(13):1202-1208. doi:10.1212/WNL.0B013E3182897103

104. Betts MJ, Cardenas-Blanco A, Kanowski M, et al. Locus coeruleus MRI contrast is reduced in Alzheimer's disease dementia and correlates with CSF Aβ levels. *Alzheimer's Dement Diagnosis, Assess Dis Monit*. 2019;11:281-285. doi:10.1016/J.DADM.2019.02.001

105. Chan-Palay V, Asan E. Quantitation of catecholamine neurons in the locus coeruleus in human brains of normal young and older adults and in depression. *J Comp Neurol*. 1989;287(3):357-372. doi:10.1002/CNE.902870307

106. Szot P, Franklin A, Miguelez C, et al. Depressive-like behavior observed with a minimal loss of locus coeruleus (LC) neurons following administration of 6-hydroxydopamine is associated with electrophysiological changes and reversed with precursors of norepinephrine. *Neuropharmacology*. 2016;101:76-86. doi:10.1016/J.NEUROPHARM.2015.09.003

107. del Cerro I, Martínez-Zalacaín I, Guinea-Izquierdo A, et al. Locus coeruleus connectivity alterations in late-life major depressive disorder during a visual oddball task. *NeuroImage Clin*. 2020;28:102482. doi:10.1016/J.NICL.2020.102482

108. Wang J, Li Y, Huang Z, et al. Neuromelanin-sensitive magnetic resonance imaging features of the substantia nigra and locus coeruleus in de novo Parkinson's disease and its phenotypes. *Eur J Neurol*. 2018;25(7):949-e73. doi:10.1111/ENE.13628

109. Aarsland D, Påhlhagen S, Ballard CG, Ehrt U, Svenningsson P. Depression in Parkinson disease - Epidemiology, mechanisms and management. *Nat Rev Neurol*. 2012;8(1):35-47. doi:10.1038/nrneurol.2011.189

110. Bohnen NI, Kaufer DI, Hendrickson R, Constantine GM, Mathis CA, Moore RY. Cortical cholinergic denervation is associated with depressive symptoms in Parkinson's disease and parkinsonian dementia. *J Neurol Neurosurg Psychiatry*. 2007;78(6):641-643. doi:10.1136/jnnp.2006.100073

111. Fetoni V, Soliveri P, Monza D, Testa D, Girotti F. Affective symptoms in multiple system atrophy and Parkinson's disease: response to levodopa therapy. *J Neurol Neurosurg Psychiatry*. 1999;66(4):541-544. doi:10.1136/JNNP.66.4.541

112. Herting B, Beuthien-Baumann B, Pöttrich K, et al. Prefrontal cortex dysfunction and depression in atypical parkinsonian syndromes. *Mov Disord*. 2007;22(4):490-497. doi:10.1002/MDS.21237

113. Boeve BF, Silber MH, Saper CB, et al. Pathophysiology of REM sleep behaviour disorder and relevance to neurodegenerative disease. *Brain*. 2007;130(11):2770-2788. doi:10.1093/brain/awm056

114. Iranzo A. The REM sleep circuit and how its impairment leads to REM sleep behavior disorder. *Cell Tissue Res*. 2018;373(1):245-266. doi:10.1007/S00441-018-2852-

8/FIGURES/1

115. Garcia SV, Libourel PA, Lazarus M, Grassi D, Luppi PH, Fort P. Genetic inactivation of glutamate neurons in the rat sublaterodorsal tegmental nucleus recapitulates REM sleep behaviour disorder. *Brain*. 2017;140(2):414-428. doi:10.1093/BRAIN/AWW310

116. Westlund KN, Dan Coulter J. Descending projections of the locus coeruleus and subcoeruleus/medial parabrachial nuclei in monkey: Axonal transport studies and dopamine-β-hydroxylase immunocytochemistry. *Brain Res Rev*. 1980;2(1-3):235-264. doi:10.1016/0165-0173(80)90009-0

117. Baker KG, Tork I, Hornung JP, Halasz P. The human locus coeruleus complex: an immunohistochemical and three dimensional reconstruction study. *Exp Brain Res*. 1989;77(2):257-270. doi:10.1007/BF00274983

118. Braak H, Rüb U, Sandmann-Keil D, et al. Parkinson's disease: affection of brain stem nuclei controlling premotor and motor neurons of the somatomotor system. *Acta Neuropathol*. 2000;99(5):489-495. doi:10.1007/s004010051150

119. Ehrminger M, Latimier A, Pyatigorskaya N, et al. The coeruleus/subcoeruleus complex in idiopathic rapid eye movement sleep behaviour disorder. *Brain*. 2016;139(4):1180-1188. doi:10.1093/BRAIN/AWW006

120. Sommerauer M, Fedorova TD, Hansen AK, et al. Evaluation of the noradrenergic system in Parkinson's disease: an 11C-MeNER PET and neuromelanin MRI study. *Brain*. 2018;141(2):496-504. doi:10.1093/BRAIN/AWX348

121. García-Lorenzo D, Longo-Dos Santos C, Ewenczyk C, et al. The coeruleus/subcoeruleus complex in rapid eye movement sleep behaviour disorders in Parkinson's disease. *Brain*. 2013;136(7):2120-2129. doi:10.1093/BRAIN/AWT152

122. Yao ST, Finkelstein DI, Lawrence AJ. Nitrergic stimulation of the locus coeruleus

modulates blood pressure and heart rate in the anaesthetized rat. *Neuroscience*. 1999;91(2):621-629. doi:10.1016/S0306-4522(98)00661-7

123. Schocke MFH, Seppi K, Esterhammer R, et al. Trace of diffusion tensor differentiates the Parkinson variant of multiple system atrophy and Parkinson's disease. *Neuroimage*. 2004;21(4):1443-1451. doi:10.1016/j.neuroimage.2003.12.005

124. Shiga K, Yamada K, Yoshikawa K, Mizuno T, Nishimura T, Nakagawa M. Local tissue anisotropy decreases in cerebellopetal fibers and pyramidal tract in multiple system atrophy. *J Neurol*. 2005;252(5):589-596. doi:10.1007/s00415-005-0708-0

125. Chougar L, Faouzi J, Pyatigorskaya N, et al. Automated Categorization of Parkinsonian Syndromes Using Magnetic Resonance Imaging in a Clinical Setting. *Mov Disord*. 2021;36(2):460-470. doi:10.1002/mds.28348

126. Singer W, Berini SE, Sandroni P, et al. Pure autonomic failure. *Neurology*. 2017;88(12):1129-1136. doi:10.1212/WNL.0000000000003737

127. Kaufmann H, Norcliffe-Kaufmann L, Palma JA, et al. Natural history of pure autonomic failure: A United States prospective cohort. *Ann Neurol*. 2017;81(2):287-297. doi:10.1002/ANA.24877

128. Hansson O, Janelidze S, Hall S, et al. Blood-based NfL: A biomarker for differential diagnosis of parkinsonian disorder. *Neurology*. 2017;88(10):930-937. doi:10.1212/WNL.0000000000003680

129. Marques TM, Van Rumund A, Oeckl P, et al. Serum NFL discriminates Parkinson disease from atypical parkinsonisms. *Neurology*. 2019;92(13):E1479-E1486. doi:10.1212/WNL.0000000000007179

130. Ge F, Ding J, Liu Y, Lin H, Chang T. Cerebrospinal fluid NFL in the differential diagnosis of parkinsonian disorders: A meta-analysis. *Neurosci Lett*. 2018;685:35-41.

doi:10.1016/J.NEULET.2018.07.030

131. Constantinides VC, Paraskevas GP, Emmanouilidou E, et al. CSF biomarkers β-amyloid, tau proteins and a-synuclein in the differential diagnosis of Parkinson-plus syndromes. *J Neurol Sci*. 2017;382:91-95. doi:10.1016/J.JNS.2017.09.039

132. Mondello S, Constantinescu R, Zetterberg H, Andreasson U, Holmberg B, Jeromin A. CSF α-synuclein and UCH-L1 levels in Parkinson's disease and atypical parkinsonian disorders. *Parkinsonism Relat Disord*. 2014;20(4):382-387. doi:10.1016/J.PARKRELDIS.2014.01.011

133. Shahnawaz M, Tokuda T, Waraga M, et al. Development of a Biochemical Diagnosis of Parkinson Disease by Detection of α-Synuclein Misfolded Aggregates in Cerebrospinal Fluid. *JAMA Neurol*. 2017;74(2):163-172. doi:10.1001/JAMANEUROL.2016.4547

134. Shahnawaz M, Mukherjee A, Pritzkow S, et al. Discriminating α-synuclein strains in Parkinson's disease and multiple system atrophy. *Nat 2020 5787794*. 2020;578(7794):273-277. doi:10.1038/s41586-020-1984-7

135. Singer W, Schmeichel AM, Shahnawaz M, et al. Alpha-Synuclein Oligomers and Neurofilament Light Chain in Spinal Fluid Differentiate Multiple System Atrophy from Lewy Body Synucleinopathies. *Ann Neurol*. 2020;88(3):503-512. doi:10.1002/ANA.25824

136. Quadalti C, Calandra-Buonaura G, Baiardi S, et al. Neurofilament light chain and α-synuclein RT-QuIC as differential diagnostic biomarkers in parkinsonisms and related syndromes. *NPJ Park Dis*. 2021;7(1). doi:10.1038/S41531-021-00232-4

137. Rossi M, Candelise N, Baiardi S, et al. Ultrasensitive RT-QuIC assay with high sensitivity and specificity for Lewy body-associated synucleinopathies. *Acta*

Neuropathol. 2020;140(1):49-62. doi:10.1007/S00401-020-02160-8/FIGURES/3

138. Rae CL, Davies G, Garfinkel SN, et al. Deficits in Neurite Density Underlie White Matter Structure Abnormalities in First-Episode Psychosis. *Biol Psychiatry*. 2017;82(10):716-725. doi:10.1016/J.BIOPSYCH.2017.02.008

Tables

Table 1. Common terms and parameters used in diffusion magnetic resonance imaging.

DWI	Diffusion-Weighted imaging. *Please refer to text*.
DTI	Diffusion Tensor Imaging. *Please refer to text*.
DKI	*Diffusion Kurtosis Imaging*. Diffusion MRI technique that allows to quantify the non-Gaussian diffusion (i.e. diffusional kurtosis) of water molecules. This is opposed to classical diffusion imaging, in which water diffusion is estimated through a Gaussian function (i.e. Gaussian diffusion). This modelling is conceived to take into account the presence of tissue barriers and compartments that alter the Gaussian diffusion of water. *Mean, radial and axial kurtosis* (MK, RK, AK) are specific parameters extracted from this imaging technique. At least two shells (non-zero b-values) are required during scan acquisition.
ADC	*Apparent Diffusion Coefficient*. Numerical value expressing the degree of diffusion along one axis in a voxel. The coefficient is a function of signal intensity at b=0 and b>0 and of the two b-values. The ADC map is the image resulting from the ADC values in each voxel. *Regional ADC* (*rADC*) values can be used to estimate the average ADC in a brain region.
Trace(D)	*Trace of the tensor* (the tensor is indicated by the letter *D*). Parameter obtained by the sum of ADC parameters in three orthogonal directions (x, y, z); the trace image contrast is insensitive to the orientation-effect, as opposed to the ADC obtained by scanning with a gradient applied in only one direction. The term "trace" comes from matrix algebra (since the tensor D is a 3x3 matrix) and indicates the sum of the diagonal elements of the matrix (in this case the diffusion rates along x, y and z). Of note, the average trace of a voxel, i.e. the sum of the water molecular diffusion rates along x, y and z divided by 3, is equal to the Mean Diffusivity (MD).
FA	*Fractional anisotropy*. Measure of the degree of diffusion anisotropy (propensity of water molecules to diffuse along a preferential axis). This value ranges between 0 (isotropic diffusion) and 1 (anisotropic diffusion).
MD, AD, RD	*Mean Diffusivity*: overall measure of diffusion in a voxel or region. *Axial Diffusivity*: measure of diffusion along the main axis of diffusion. *Radial Diffusivity*: average measure of diffusion along the two minor axes of diffusion.
FW	*Free Water*: this measure aims to provide an accurate description of brain tissue where more than one diffusion compartment is present. This is conceptually based on a two-compartment model and calculation of this parameter requires a bi-tensor model, as opposed to single-tensor model (and single-compartment) used for estimating FA and diffusivity. Free-water-corrected diffusion parameters (FA) may also be calculated.
NODDI	*Neurite Orientation Dispersion and Density Imaging*. Diffusion MRI technique based on a three-compartment tissue model. The tissue is conceptually divided in an intra-neurite, an extra-neurite and a freely-diffusing water compartments. Resulting parameters are the *orientation dispersion index* (*ODI*, an index of orientation coherence of neurites), *the neurite density index or intracellular volume fraction* (*NDI or ICvf*, an index that quantifies the packing density of axons and dendrites), and *isotropic volume fraction* (ISOvf, or free water fraction, which estimates the degree of CSF contamination). At least two shells (i.e. non-zero b-values) are required for this imaging technique.
TBSS	*Tract-Based Spatial Statistics*, an automated, observer-independent approach for assessing fractional anisotropy in white matter tracts on a voxel-wise basis across groups, overcoming common issues in FA comparison between subjects (i.e.

	registration to a common space and spatial smoothing).

Table 2. Demographics and general clinical characteristics of the study population.

	Healthy controls (HC)	**Parkinson's Disease (PD)**	**Multiple system atrophy (MSA)**
Number of patients, n	18	19	11 (7 P, 4 C)
Age, median (IQR, range)	59 (19, 46-79)	64 (12, 47-79)	64 (11, 56-79)
Sex (M/F)	7/11	12/7	6/5
Duration of symptoms, median	-	7 (7, 1-11)	3 (2, 1-6)
MDS-UPDRS I, median (IQR, range)	-	10 (9, 0-22)	15 (12, 7-25)
MDS-UPDRS II, median (IQR, range)	-	7 (8, 1-21)	20 (8, 11-41)
MDS-UPDRS III, median (IQR, range)	-	32 (21, 15-64)	-
UMSARS I, median (IQR, range)	-	-	18 (7, 13-36)
UMSARS II, median (IQR, range)	-	-	27 (12, 19-38)
Hoehn and Yahr, median (IQR, range)	-	2 (0, 1-4)	-
RBDSQ, median (IQR, range)	1 (3, 0-4)	4 (7, 1-13)	6 (10, 1-11)
MoCA, median (IQR, range)	-	27 (4, 24-30)	25 (3, 21-29)
MMSE, median (IQR, range)	30 (2, 26-30)	29 (2, 26-30)	29 (2, 24-30)
HADS total, median (IQR, range)	-	6 (10, 1-20)	16 (10, 8-34)
SCOPA-AUT, median (IQR, range)	-	11 (12, 0-22)	25 (16, 11-52)
NMS-QUEST, median (IQR, range)	-	8 (9, 0-19)	15 (6, 6-19)
SCOPA-PS, median (IQR, range)	-	4 (7, 0-23)	19 (11, 5-28)

Abbreviations. HADS: Hospital Anxiety and Depression Scale; IQR: interquartile range; MDS-UPDRS: Movement Disorders Society – Unified Parkinson's Disease Rating Scale; MoCA: Montreal Cognitive Assessment; MMSE: Mini Mental State Examination; n: number of patients; NMS-QUEST: Non-Motor Symptoms Questionnaire; RBDSQ: Rapid Eye Movement Sleep Disorder Questionnaire; SCOPA-AUT: Scales for Outcomes in Parkinson's Disease – Autonomic; SCOPA-psych: Scales for Outcomes in Parkinson's Disease – Psychosocial functioning; UMSARS: Unified Multiple System Atrophy Rating Scale.

Table 3. Neuromelanin and NODDI parameters in anterior and posterior substantia nigra (SN). Neuromelanin content was estimated as volume of voxels exceeding +3.25 standard deviations of the mean background intensity (cerebral peduncles).

Site	**Parameter**	**HC (n=18)** Mean (SD)	**PD (n=19)** Mean (SD)	**MSA (n=11)** Mean (SD)
Anterior SN	Neuromelanin	83.03 (31.11)	61.90 (33.81)	52.94 (30.77)
	NDI	0.7978 (0.0836)	0.8281 (0.0667)	0.8648 (0.0742)
	FWF	0.0803 (0.0687)	0.0705 (0.0563)	0.1305 (0.1109)
	ODI	0.2602 (0.0572)	0.2878 (0.0505)	0.2783 (0.0591)
Posterior SN	Neuromelanin	28.86 (12.41)	15.85 (13.13)	16.00 (9.72)
	NDI	0.7200 (0.0856)	0.7703 (0.1044)	0.8081 (0.0705)
	FWF	0.0719 (0.0649)	0.1426 (0.1136)	0.1858 (0.1209)
	ODI	0.2494 (0.0472)	0.2718 (0.0287)	0.2766 (0.0455)

Abbreviations. FWF: free water fraction; HC: healthy controls; MSA: multiple system atrophy; NDI: neurite density index; ODI: orientation dispersion index; PD: Parkinson's disease.

Table 4. Diffusion MRI values extracted from the neurite orientation and dispersion density imaging (NODDI) from selected locations in Parkinson's Disease and Multiple System Atrophy.

		PD (n=19) Mean (SD)	**MSA, (n=11)** Mean (SD)	**Mann Whitney U**	**p-value**
Putamen	**FWF**	0.04409 (0.03455)	0.11250 (0.09533)	145.0	0.021
	ODI	0.52987 (0.03129)	0.53129 (0.03551)	49.0	0.035
Caudate	**FWF**	0.00619 (0.00663)	0.01399 (0.00741)	154.0	0.006
	ODI	0.47377 (0.04186)	0.49552 (0.03979)	121.0	0.247
Pallidum	**FWF**	0.11717 (0.10180)	0.16917 (0.14369)	125.0	0.179
	ODI	0.45482 (0.03196)	0.44650 (0.03252)	85.0	0.668
Cerebellar grey matter (lobule VI)	**FWF**	0.02823 (0.03323)	0.11247 (0.11051)	146.0	0.019
	ODI	0.47289 (0.03430)	0.49726 (0.02991)	135.0	0.069
MCP	**NDI**	0.79654 (0.04182)	0.70095 (0.12417)	44.0	0.019
Cerebellar WM	**NDI**	0.82437 (0.04995)	0.73620 (0.16104)	57.0	0.085
Ventral pons (WM)	**NDI**	0.75503 (0.05571)	0.69647 (0.05979)	52.0	0.050

Abbreviations. FWF: free water fraction; MCP: middle cerebellar peduncle; MSA: Multiple system atrophy; NDI: neurite density index; ODI: orientation dispersion index; PD: Parkinson's Disease; WM: white matter.

Table 5. Relationships between locus coeruleus (LC) neuromelanin MRI contrast and non-motor symptoms scores in Multiple System Atrophy (MSA) and Parkinson's Disease (PD). Numbers indicate Spearman's rho correlation coefficients. Asterisks (*) flag significant correlations with $p < 0.05$, uncorrected (p-values are reported in the main text).

	Rostral LC		**Intermediate LC**		**Caudal LC**	
	MSA	**PD**	**MSA**	**PD**	**MSA**	**PD**
MoCA	0.770*	0.105	0.567	0.394	0.161	-0.192
HADS-D	-0.664*	-0.372	-0.389	-0.215	0.334	-0.056
RBDSQ	-0.606*	-0.006	-0.592	-0.137	0.321	0.129
SCOPA-sleep	0.393	0.109	0.142	-0.004	0.005	-0.191

Abbreviations. HADS-D: Hospital Anxiety and Depression Scale – Depression subscore; MoCA: Montreal Cognitive Assessment; RBDSQ: Rapid Eye Movement Sleep Disorder Questionnaire; SCOPA-sleep: Scales for Outcomes in Parkinson's Disease – sleep.

Figures

Figure 1. Schematic representation of the Neurite Orientation Dispersion and Density Imaging (NODDI) tissue modelling, and how it differs from diffusion tensor imaging (DTI). DTI models tissue with a diffusion tensor (a 3x3 matrix geometrically resembling an ellipsoid in space), through which mean diffusivity (MD) and fractional anisotropy (FA) can be estimated. NODDI models brain tissue in three compartments: intra-neurite, extra-neurite, and cerebrospinal fluid (CSF) compartments. This is achieved by applying a two-level approach to separate the volume fraction of Gaussian isotropic diffusion (free water fraction, FWF), representing freely diffusing water (i.e. CSF), from the neural tissue. The remaining signal is compartmentalised into non-exchanging intra and extra-neurite water. Parameter maps of neurite density index (NDI), representing mainly the intracellular compartment, free water fraction (FWF), representing freely diffusing water, and orientation dispersion index (ODI), representing neurites orientation dispersion in space, can be estimated. Yellow circles highlight a region containing all three tissue components, i.e. CSF, grey matter and white matter, and how it would be interpreted by the different models. Reproduced with permission from Rae et al., 2017.[138]

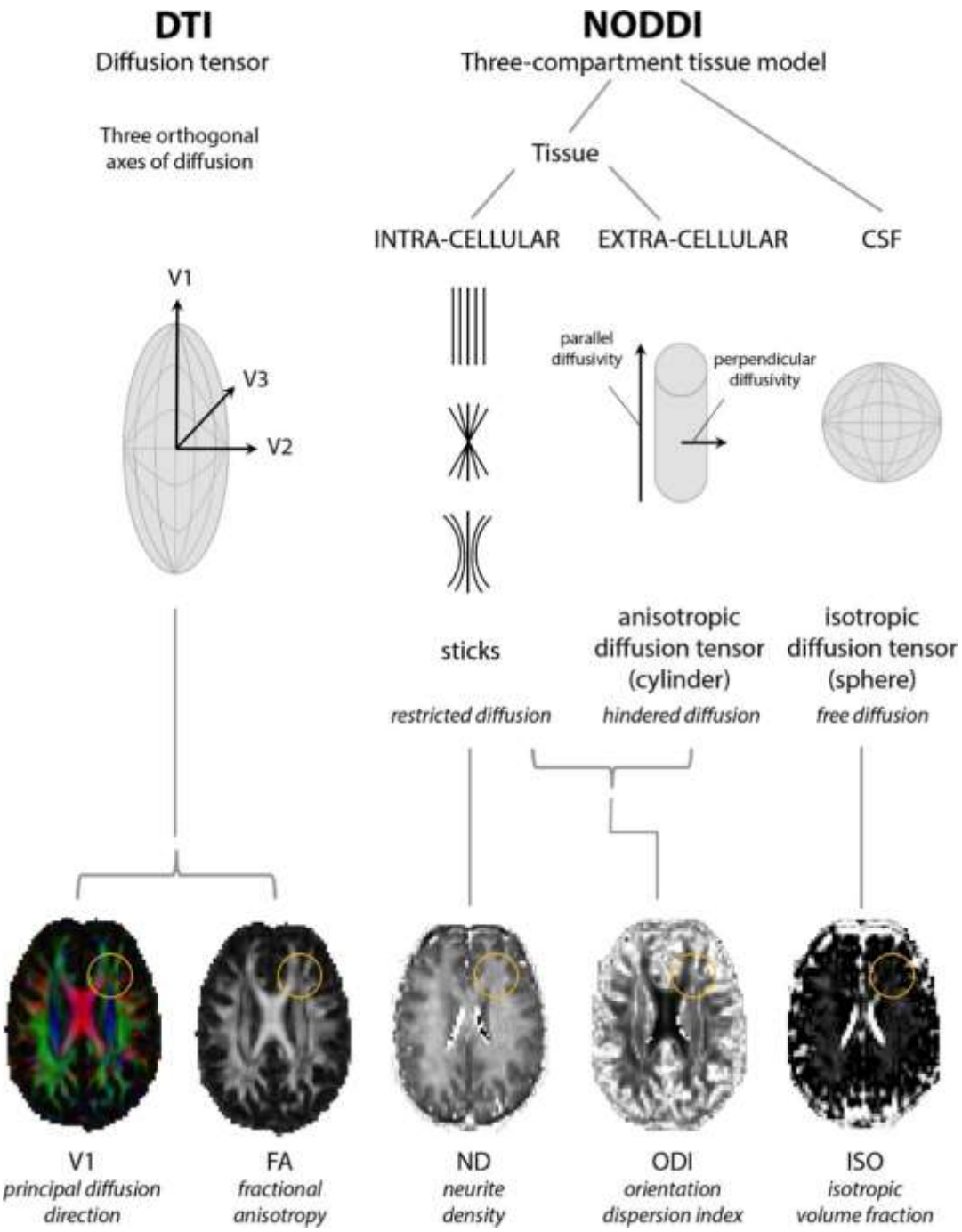
DTI
Diffusion tensor
Three orthogonal axes of diffusion
V1
V3
V2
NODDI
Three-compartment tissue model
Tissue
INTRA-CELLULAR
EXTRA-CELLULAR
CSF
parallel diffusivity
perpendicular diffusivity
sticks
anisotropic diffusion tensor (cylinder)
isotropic diffusion tensor (sphere)
restricted diffusion
hindered diffusion
free diffusion
V1
principal diffusion direction
FA
fractional anisotropy
ND
neurite density
ODI
orientation dispersion index
ISO
isotropic volume fraction

Figure 2. Regions of interest (ROIs) placed on the diffusion MRI template. ROIs were placed onto: middle cerebellar peduncles (MCPs), ventral pons white matter tracts, cerebellar white matter and cerebellar lobule VI grey matter (not shown) (first row); putamen, pallidum, caudate (second row); anterior and posterior substantia nigra (SN) (third row). To ensure correct placing of the SN ROIs a template image from the gradient echo magnetization transfer (neuromelanin-sensitive) images was created and transformed to diffusion template space; the third row shows the midbrain from the diffusion template with superimposed SN hyperintensity derived from the neuromelanin image template.

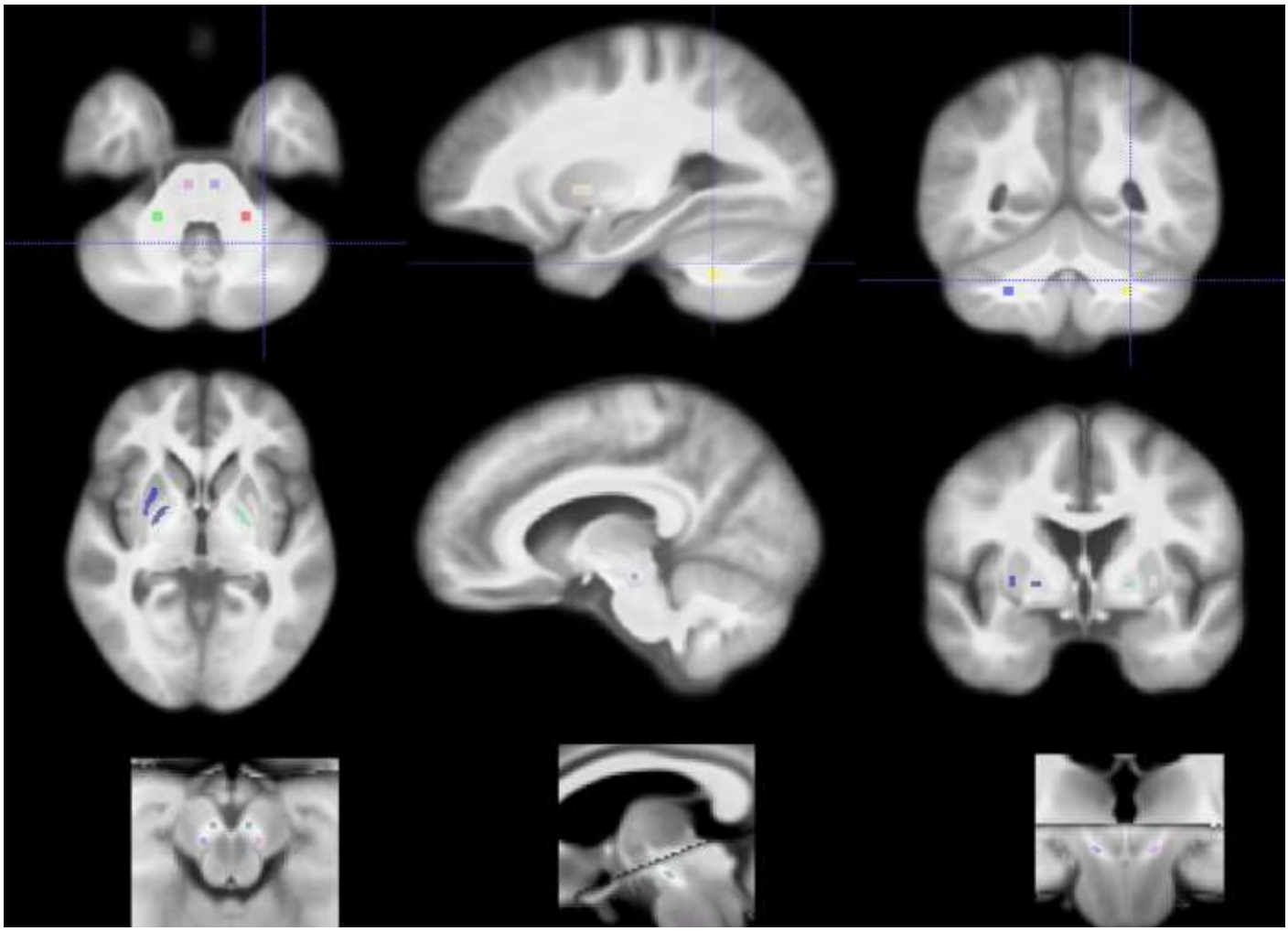

Figure 3. (A) shows the relationship between substantia nigra (SN) neurite density index (NDI) and free water fraction (FWF) is shown. (B) shows the relationship between SN NDI and neuromelanin content. Linear fit lines for each subgroup and total linear fit lines are also shown.

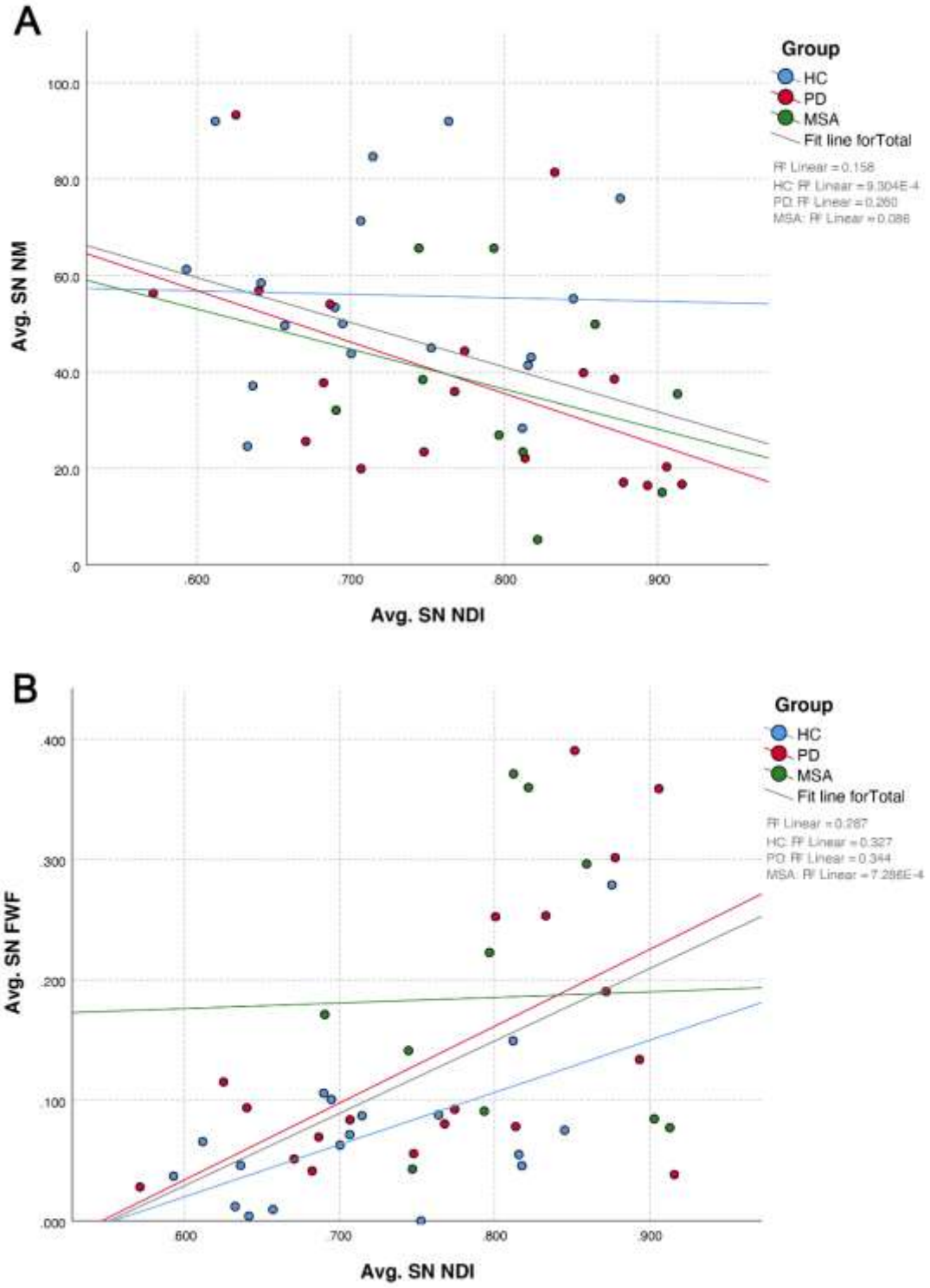

Figure 4. Mean MRI contrast and 95% confidence interval (CI) in the entire locus coeruleus (LC) and in its rostral, intermediate and caudal subportions in Healthy Controls (HC), Parkinson's Disease (PD) and Multiple System Atrophy (MSA) patients.

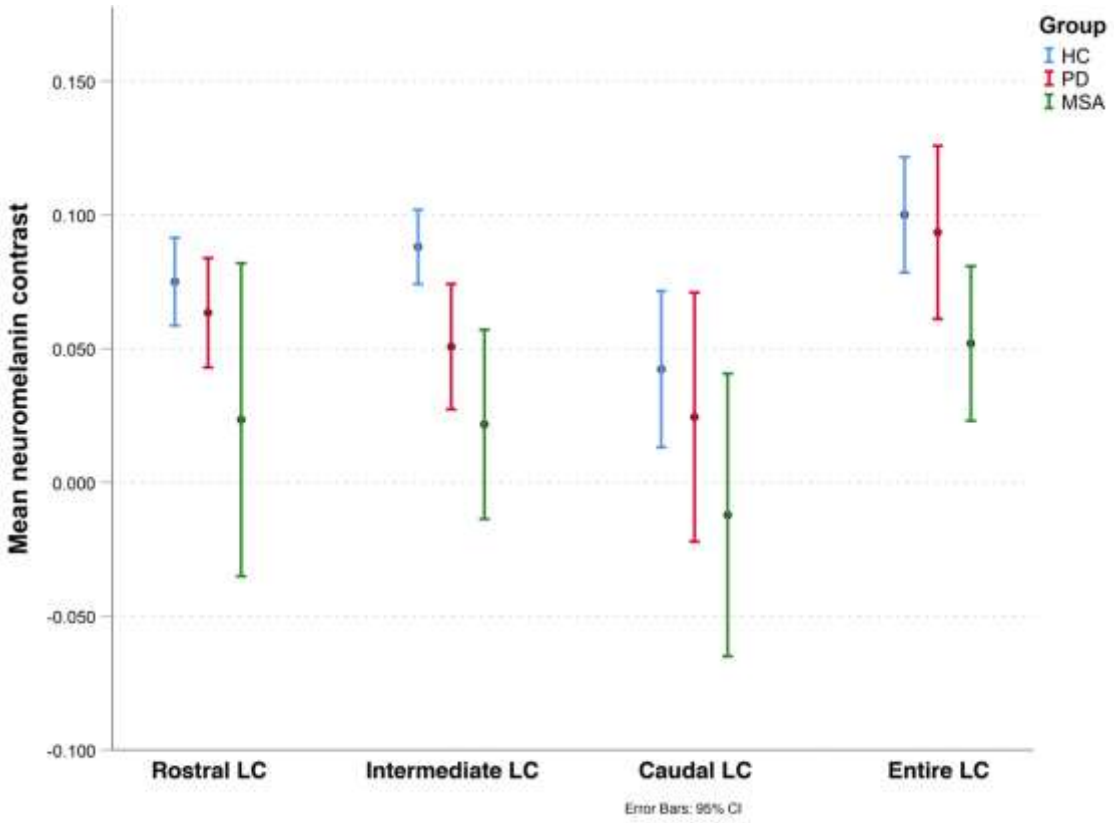

Figure 5. 3D scatterplot representing the relationship between Montreal Cognitive Assessment (MoCA) scores, rostral locus coeruleus (LC) neuromelanin (NM) content and anterior substantia nigra (SN) neuromelanin content in Parkinson's Disease (PD) and Multiple System Atrophy (MSA) patients. The regression plane highlights a direct association between MoCA scores and both rostral LC and anterior SN. The plane was modelled through a linear model as $y \sim x + z$. The dotted line along the yz plane represents the relationship between MoCA scores and average rostral LC neuromelanin content; the dotted line along the xy plane represents the relationship between MoCA scores and average anterior SN neuromelanin content.

Abbreviations: Avg.: average; LC: Locus coeruleus; MoCA: Montreal Cognitive Assessment; MSA: Multiple System Atrophy; NM: neuromelanin; PD: Parkinson's Disease.